Atmospheric
Chemistry
and Physics

Vertical variability of aerosol properties and trace gases over a remote marine region: a case study over Bermuda

Taiwo Ajayi[1], Yonghoon Choi[2], Ewan C. Crosbie[2,3], Joshua P. DiGangi[2], Glenn S. Diskin[2],
Marta A. Fenn[2,3], Richard A. Ferrare[2], Johnathan W. Hair[2], Miguel Ricardo A. Hilario[1],
Chris A. Hostetler[2], Simon Kirschler[4], Richard H. Moore[2], Taylor J. Shingler[2], Michael A. Shook[2],
Cassidy Soloff[1], Kenneth L. Thornhill[2], Christiane Voigt[4,5], Edward L. Winstead[2,3], Luke D. Ziemba[2],
and Armin Sorooshian[1,6]

[1]Department of Hydrology and Atmospheric Sciences, University of Arizona, Tucson, AZ 85721, USA
[2]NASA Langley Research Center, Hampton, VA 23681, USA
[3]Analytical Mechanics Associates, Hampton, VA 23666, USA
[4]Department of Cloud Physics and Traffic Meteorology, Institute of Atmospheric Physics,
German Aerospace Center, Oberpfaffenhofen-Wessling, Germany
[5]Department of Atmospheric Physics, Institute of Atmospheric Physics, University of Mainz, Mainz, Germany
[6]Department of Chemical and Environmental Engineering, University of Arizona, Tucson, AZ 85721, USA

Correspondence: Armin Sorooshian (armin@arizona.edu)

Abstract. Remote marine regions comprise a high fraction of Earth's surface, but in situ vertically resolved measurements over these locations remain scarce. Here we use airborne data during 15 vertical spiral soundings (0.15–8.5 km) over Bermuda during the NASA Aerosol Cloud meTeorology Interactions over the western ATlantic Experiment (ACTIVATE) to investigate the impact of different source regions on the vertical structure of trace gases, aerosol particles, and meteorological variables over 1000 km offshore of the US East Coast. Results reveal significant differences in vertical profiles of variables between three different air mass source categories (North America, Ocean, Caribbean/North Africa) identified using the Hybrid Single-Particle Lagrangian Integrated Trajectory (HYSPLIT) model: (i) the strongest pollution signature is from air masses from the North America category, while the weakest one is from the Ocean category; (ii) North America air has the highest levels of CO, CH_4, submicron particle number concentration, aerosol mass spectrometer (AMS) mass, and organic mass fraction along with smoke layers in the free troposphere (FT); (iii) Ocean air has the highest relative amount of nitrate, non-sea-salt sulfate, and oxalate, which are key acidic species participating in chloride depletion; (iv) air masses from the Caribbean/North Africa showed a pronounced coarse aerosol signature in the FT and reduced aerosol hygroscopicity, which is associated with dust transport; and (v) there is considerable vertical heterogeneity for almost all variables examined, including higher O_3 and submicron particle concentrations with altitude, suggesting that the FT is a potential contributor of both constituents in the marine boundary layer. This study highlights the importance of considering air mass source origin and vertical resolution to capture aerosol and trace gas properties over remote marine areas.

1 Introduction

Atmospheric studies are important to conduct over oceans, which represent a large fraction of Earth's surface area. Remote marine areas are particularly important because sometimes they represent cleaner conditions with lower aerosol number concentrations, and clouds under such clean conditions account for much of the diversity in observational and model calculations for radiative forcing from aerosol–cloud interactions (Gryspeerdt et al., 2023). While it may seem reasonable to assume that such clean conditions are more attainable far away from continents (> 1000 km), such remote areas may not be clean due to long-range transport. Even if the atmosphere is not pristine at such offshore distances, characterizing such environments is helpful for comparisons to reanalysis, remote sensing, and model output data. In particular, vertically resolved in situ data for aerosol properties and trace gases are difficult to obtain over remote marine areas, which presents challenges for validation and improvement of models and reanalysis products (Easter et al., 2004; Edwards et al., 2022; Fernandes et al., 2023) since past work has shown significant deviations in aerosol properties at the surface versus higher levels that are more relevant for clouds (Pringle et al., 2010). Such data from airborne platforms are necessary for better determining how the vertical distribution of particles and trace gases impacts atmospheric processes such as cloud lifecycle and radiative transfer.

The island of Bermuda in the northwestern Atlantic is more than 1000 km from the US East Coast and receives transported emissions from multiple continents, such as North and Central America, Asia, Europe, and Africa (Holben et al., 2001; Smirnov et al., 2002). This blend of seasonally dependent continental sources and marine emissions has drawn researchers to Bermuda and the adjacent Sargasso Sea for decades (e.g., Wolff et al., 1986; Galloway et al., 1989; Moody et al., 1995; Anderson et al., 1996; Arimoto et al., 2003; Keene et al., 2014; Aldhaif et al., 2021). Table S1 in the Supplement summarizes the rich body of past studies conducted at Bermuda. While much is known about the surface characteristics of trace gases and aerosol particles at Bermuda, much less is known aloft, with the exception of a few studies which compare aerosol size distribution characteristics in the boundary layer and free troposphere, showing higher number and volume concentrations (and the associated mean diameters of number and volume) at lower altitudes (Horvath et al., 1990; Kim et al., 1990). There are knowledge gaps for other aerosol properties (e.g., new particle formation, aerosol composition, hygroscopicity, and optical properties) and trace gases, especially as this relates to their vertical distribution and sensitivity to air mass source regions. Aryal et al. (2014) showed that surface optical data were weakly related to column optical properties over Bermuda, strongly motivating more meticulous examination above the surface, where there can be heterogeneity in gas and aerosol characteristics.

The goal of this work is to use a series of aircraft vertical spiral soundings conducted around Bermuda during the NASA Aerosol Cloud meTeorology Interactions oVer the western ATlantic Experiment (ACTIVATE) airborne mission to characterize the vertical distribution of aerosol particle characteristics and trace gas levels. We also examine differences in the measurement data between the boundary layer and free troposphere as a function of air mass source. Section 2 summarizes the ACTIVATE field campaign measurements used in this work along with the calculation methods. Section 3 presents the results and a discussion. Section 4 provides the conclusions. To aid with the paper, Table S2 in the Supplement provides definitions of acronyms and abbreviations used subsequently.

2 Methods

2.1 Flight campaign

The NASA ACTIVATE campaign involved 3 years of flights with separate deployments each year in the winter and summer months (Sorooshian et al., 2019, 2023). ACTIVATE involved two NASA Langley Research Center (LaRC) aircraft flying in spatial coordination. A HU-25 Falcon flew in and above the marine boundary layer (usually < 3 km), while a King Air flew at around ~ 9 km. The Falcon conducted in situ measurements of trace gases, aerosol particles, meteorological variables, and clouds, while King Air carried out remote sensing and launched dropsondes. Flights were mostly based out of NASA LaRC in Hampton, Virginia, with durations of < 4 h. Due to restrictions associated with the COVID-19 pandemic, the possibility of flying to Bermuda only opened up in the final deployment (summer 2022), prompting the mission team to conduct an intensive operation based at L. F. Wade International Airport (Bermuda) between 31 May and 18 June 2022; this period included research flights 161–179, with the first and last in this group being transit flights back and forth from Virginia to Bermuda. The objective in the current study is a detailed examination of data collected from a total of 15 vertical spiral soundings (~ 0.15 to as high as ~ 8 km) with the HU-25 Falcon during the Bermuda intensive period (details in Table 1 and locations in Fig. 1). Most of the Falcon spirals were coordinated with King Air such that the latter would fly over the Falcon's spiral location to provide vertically resolved profiles of aerosol properties.

2.2 Instrumentation

Table 2 summarizes instrumentation details relevant to this study on both the Falcon and King Air with a brief description provided below. Extensive details regarding all ACTIVATE flights and instruments are provided elsewhere (Sorooshian et al., 2023). Beginning with in situ measurements on the Falcon, a PICARRO G2401-m instrument measured CO, CO_2, and CH_4, while the 2B Tech. Inc. Model 205

Table 1. Summary of details relevant to the 15 Falcon spiral soundings used in this study. APT means accumulated precipitation along trajectories ending at the location of the Falcon (described in Sect. 2.3). MBLH: calculated marine boundary layer height from Falcon data (Sect. 2.4.2); MLH: HSRL-2-derived values of aerosol mixed layer height ("NA" means no data were available during the portion of the flight over the location of the Falcon's spiral sounding).

Research flight – date	Spiral stop and start times (UTC)	Altitude range (m)	Falcon MBLH/HSRL-2 MLH (m)	APT (mm)	Air mass source category
162 – 06/02/2022	12:58–13:10	150–4000	1050/NA	3.23	Ocean
162 – 06/02/2022	13:48–14:10	150–3200	1050/NA	2.67	Ocean
163 – 06/02/2022	18:36–18:53	150–4000	750/NA	2.18	Ocean
166 – 06/07/2022	14:32–14:47	150–3200	950/945	0.67	North America
167 – 06/07/2022	19:08–19:23	150–3500	1200/1100	0.45	North America
168 – 06/08/2022	20:30–20:45	150–4000	1250/1100	0.07	North America
169 – 06/10/2022	15:17–15:25	150–3500	800/NA	7.14	Caribbean/North Africa
169 – 06/10/2022	19:30–19:51	150–5000	800/700	7.60	Caribbean/North Africa
170 – 06/10/2022	20:25–20:35	150–5000	1190/NA	8.73	Caribbean/North Africa
171 – 06/11/2022	15:24–15:42	150–5000	1190/NA	6.16	Caribbean/North Africa
172 – 06/11/2022	20:08–20:30	150–3000	1350/1110	6.14	Caribbean/North Africa
173 – 06/13/2022	14:30–14:46	150–4500	805/815	2.12	Caribbean/North Africa
174 – 06/13/2022	19:46–20:09	150–4500	915/940	2.65	Caribbean/North Africa
176 – 06/14/2022	16:05–16:25	150–8500	1210/1240	3.14	Caribbean/North Africa
178 – 06/17/2022	16:20–16:47	150–7600	1210/1230	9.67	North America

instrument measured O_3. The Picarro G2401-m sampled air via an air temperature probe (Buck Research Instruments, LLC) on the aircraft's crown next to the aerosol inlets. Calibrations were conducted hourly during flights and weekly on the ground. Ozone measurements relied on using a forward-facing J-probe inlet on the HU-25 Falcon nadir panel with a specialized sampling device to increase data quality at high altitudes. Data quality checks were conducted hourly during flight, such as zeroing for 1 min using a KI filter. Water vapor measurements were conducted with a diode laser hygrometer (DLH), which is an open-path, near-infrared absorption spectrometer. Its optical path was outside the aircraft between an aircraft window and a retroreflector on a starboard wing pylon.

Aerosol number concentrations in different size ranges were measured with multiple condensation particle counters, and size distributions extending from 3 to 5000 nm were obtained with a scanning mobility particle sizer (SMPS; 3–100 nm) and a laser aerosol spectrometer (LAS; 100–5000 nm). The SMPS categorizes particles according to their electrical mobility diameters, while the LAS categorizes them based on their optical diameters (Sorooshian et al., 2023). The LAS is calibrated using monodisperse ammonium sulfate particles since they have a refractive index (1.52) representative of ambient aerosol particles (Shingler et al., 2016a, b; Aldhaif et al., 2018). The archived SMPS and LAS data are adjusted so that the SMPS electric mobility diameters match the optical diameters of the LAS, allowing size distributions from the two instruments to be stitched together (Sect. 3.5, Sorooshian et al., 2023). The stitched size distributions had fits made to them with a nonlinear

least-squares fit of a two-mode lognormal distribution using the Python package scipy.optimize.curve_fit (Virtanen et al., 2020).

The hygroscopicity parameter $f(RH)$ for submicron aerosol was measured using tandem nephelometers with relative humidities set to approximately 20 % and 80 % (Ziemba et al., 2013). Humidification was conducted with a custom-made humidifier, and the $f(RH)$ was calculated as the total light scattering (550 nm) at 80 % relative to 20 %. While optical properties were characterized (e.g., scattering, absorption), those results are the subject of separate work related to the larger dataset from flights during June 2022. The high-resolution time-of-flight aerosol mass spectrometer measured the submicron non-refractory aerosol chemical composition (DeCarlo et al., 2008), including mass concentrations of sulfate, nitrate, chloride, ammonium, and organics with a vacuum aerodynamic diameter window from 60 to 600 nm. Data were collected using a pressure-controlled inlet (500 Torr) and averaged to a 30 s time resolution using the native 1 Hz fast-MS-mode measurements. The instrument's ionization efficiency was calibrated with 400 nm ammonium nitrate particles. A collection efficiency of 1 was applied to the data after comparison to sulfate measured by the particle-into-liquid sampler (PILS) instrument, which is described subsequently. This study makes use of the spectral marker m/z 44, which signifies oxygenated organic species (Zhang et al., 2005). The ratio of m/z 44 to the total organics is referred to as f_{44} and is of interest in this study, as work from ACTIVATE (Dadashazar et al., 2022) and other regions (Sorooshian et al., 2010) shows an enhancement in this ratio that is associated with cloud processing. To allow for better
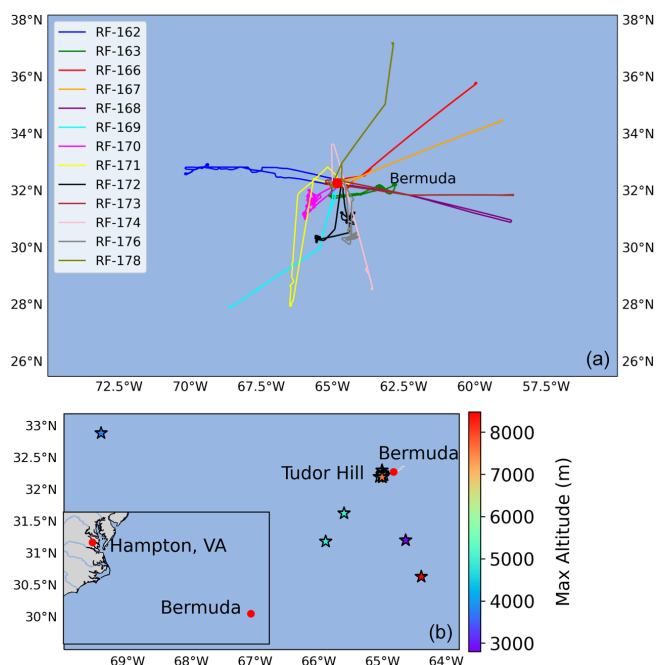
Figure 1. (a) Flight tracks corresponding to the 13 flights that included the 15 Falcon spiral soundings, colored by research flight (RF) number. Bermuda is marked with a red marker. **(b)** Location of the Falcon spiral soundings colored by the maximum altitude reached by the Falcon. The inset map shows the location of Bermuda relative to North America and the main base of operations during ACTIVATE (NASA Langley Research Center in Hampton, Virginia). Tudor Hill is labeled for context since it is an extensively used research site by the southwestern tip of Bermuda that was close to the locations of most spirals.

data quality, m/z-44 data are used when the organic mass concentration exceeded $0.4\,\mu g\,m^{-3}$.

Water-soluble aerosol composition data were collected with a PILS coupled to offline ion chromatography (IC) (Crosbie et al., 2022). The PILS–IC data are at 5 min resolution and serve to complement the aerosol mass spectrometer (AMS) data by allowing for a look at the aerosol composition up to a diameter of 5 µm, in addition to speciating tracers for sea salt (e.g., Na^+) and dust (e.g., Ca^{2+}), which is not possible with the AMS. We note that denuders were not used, and thus some species such as nitrate may be subject to artifacts. Details of the IC analysis are provided in detail elsewhere (Gonzalez et al., 2022; Corral et al., 2022b). Non-sea-salt sulfate (nss SO_4^{2-}) from the PILS–IC was calculated using the ratio of sulfate to sodium in pure seawater assuming all the sodium came from sea salt. For help with cloud screening to avoid droplet shatter artifacts, data are only used when the wing-mounted fast cloud droplet probe (FCDP; 3–50 µm diameter) measured a liquid water content (LWC) of below $0.02\,g\,m^{-3}$ and a cloud droplet number concentration of less than $10\,cm^{-3}$ (Kirschler et al., 2023). The FCDP is a forward-scattering probe on the port wing of the Falcon, with

extensive processing and corrections applied as summarized by Kirschler et al. (2022). Only 2 of the 15 spirals included a cloud layer (RF 168 on 8 June 2022 and RF 178 on 17 June 2022), which was confirmed using the Falcon's forward camera.

The higher-flying King Air obtained vertical profiles of temperature, relative humidity, and wind speed via dropsondes launched with the National Center for Atmospheric Research (NCAR) Airborne Vertical Atmospheric Profiling System (AVAPS) (Vömel et al., 2023). Dropsondes were strategically positioned within reasonable proximity to the location of the Falcon spiral soundings to offer a meaningful intercomparison. The data span from approximately 9 km to the surface, with the former being the typical flight altitude of King Air. We use vertically resolved data of the aerosol extinction, aerosol depolarization ratio, and lidar ratio as measured by the second-generation High Spectral Resolution Lidar (HSRL-2) instrument (Hair et al., 2008; Burton et al., 2018). This instrument provides vertically resolved values of aerosol backscatter and depolarization at 355, 532, and 1064 nm along with independent measurements of aerosol extinction at 355 and 532 nm using the HSRL method. Additionally, we use the aerosol mixed layer height (MLH) (Scarino et al., 2014) and aerosol type (Burton et al., 2012) products derived from the HSRL-2 base products. King Air did not fly on 2 June 2022 owing to maintenance requirements and thus did not provide data for the Ocean category, which coincidentally involved flights (RF 162–163) on just that one day.

2.3 Air mass source identification

A critical aspect of this study was to identify the source of air arriving at different vertical levels of each spiral sounding. To do this, 72 h back-trajectories were obtained using the NOAA Hybrid Single-Particle Lagrangian Integrated Trajectory model (HYSPLIT) (Stein et al., 2015; Rolph et al., 2017) arriving at different vertical levels (1 min apart) of each spiral. Although not shown, 10 d back-trajectories were also used to corroborate air mass type assignments. Trajectories were produced using the Global Data Assimilation System (GDAS, $1° \times 1°$ global resolution) archive data and the model vertical velocity approach. Additionally, accumulated precipitation along trajectories (APT) was estimated by summing up the precipitation at each 1 h time step along each trajectory to the spiral sounding location. APT is a proxy variable to represent the possibility of aerosol removal via wet scavenging along trajectory paths (Dadashazar et al., 2021; Hilario et al., 2021).

2.4 Calculations

2.4.1 Air mass source categories

HYSPLIT trajectories were divided into three categories based on the source region each trajectory spent the most

Table 2. Summary of the HU-25 Falcon and King Air instruments from which data are used in this study.

Observable	Instrument	Diameter range (µm)	Time resolution (s)	Reference
HU-25 Falcon				
Aerosol number concentration	TSI-3776 condensation particle counter (CPC)	0.003–5	1	Xiao et al. (2023)
Aerosol number concentration	TSI-3772 CPC	0.01–5	1	Xiao et al. (2023)
Dry aerosol size distribution	TSI scanning mobility particle sizer (SMPS): model 3085 Differential mobility analyzer (DMA): model 3776 CPC and model 3088 neutralizer	0.003–0.1	45	Xiao et al. (2023)
Dry aerosol size distribution	TSI 3340 laser aerosol spectrometer (LAS)	0.1–5	1	Moore et al. (2021)
$f(\mathrm{RH})$ hygroscopicity	TSI-3563 nephelometer with 80 % humidification	< 1		Ziemba et al. (2013)
Speciated non-refractory mass (SO_4^{2-}, NO_3^-, NH_4^+, Cl^-, Org, m/z 44)	Aerodyne high-resolution time-of-flight aerosol mass spectrometer (HR-ToF-AMS)	0.06–0.6	25	DeCarlo et al. (2008)
Speciated water-soluble aerosol mass	Brechtel Manufacturing Inc. (BMI) particle-into-liquid sampler (PILS) coupled to offline ion chromatography	< 5 µm	300	Crosbie et al. (2022)
Relative humidity water vapor	Diode laser hygrometer	NA	1	Diskin et al. (2002)
CH_4, CO, CO_2	PICARRO G2401-m	NA	2.5	DiGangi et al. (2021)
O_3	2B Tech. Inc. Model 205	NA	2	Wei et al. (2021)
Liquid water content (LWC) and drop concentration (N_d)	Fast cloud droplet probe (FCDP)	3–50	1	Kirschler et al. (2022)
GPS altitude, longitude, and latitude	Applanix 610 (navigational)	NA	1	Thornhill et al. (2003)
Temperature	Rosemount 102 sensor	NA	0.05	
King Air				
Temperature, relative humidity, wind speed	Vaisala NRD41 dropsonde (meteorological state)	NA		Vömel et al. (2023)
Aerosol depolarization ratio (532 nm), mixed layer height (MLH)	High Spectral Resolution Lidar (HSRL-2)	NA	10	Hair et al. (2008), Scarino et al. (2014), Burton et al. (2015)
Aerosol extinction, lidar ratio (532 nm), aerosol type	HSRL-2	NA	60	Hair et al. (2008), Burton et al. (2012)
GPS altitude, longitude, and latitude	Applanix 610 (navigational)	NA	1	Thornhill et al. (2003)

NA: not available.

time in before arriving at a distinct vertical level of individual spiral soundings. The three source regions are Caribbean/North Africa, North America, and Ocean, with the lattermost being primarily confined to the region surrounding Bermuda. Note that North African parcels generally curve around the Caribbean region (and are thus combined as one category), with possible influence also from the southeastern US on their path towards Bermuda. This is a common summertime trajectory pattern over the northwestern Atlantic (Sorooshian et al., 2020; Painemal et al., 2021). Trajectory paths ending at vertical levels in and above the boundary layer were similar for each spiral sounding, and thus assignments of air mass source origin apply to the entire column of individual spirals (Table 1).

2.4.2　Altitude categories for data analysis

We determined the marine boundary layer height (MBLH) for each spiral sounding using a well-established approach relying on the maximum vertical gradient of virtual potential temperature, specific humidity, and aerosol concentration (Seibert et al., 2000), as measured by the Falcon. Values range from 750 to 1350 m (Table 1) and are mostly similar to the HSRL-2 values of aerosol MLH that are independently derived using steep gradients in aerosol backscatter profiles (Scarino et al., 2014). To allow for easier comparison of data between spirals, a subset of results separates data into those collected below 1 km and those collected between 1 and 3.5 km as a way to simplify a look into the MBL and the free troposphere (FT) while avoiding bias in results for spirals ending at much higher maximum altitudes than others. Although three spirals only reached 3–3.2 km (one in each air mass category), we use 3.5 km to increase the range of altitudes into the FT (i.e., more statistics) for the majority of the spirals. For a more complete view of the vertical profiles, some figures additionally show the full altitude range of relevant measured variables.

3　Results

### 3.1　Air mass sources and weather characteristics

The back-trajectory results for the 15 aircraft spiral soundings reveal that the three predominant categories are Ocean (Fig. 2a–c), North America (Fig. 2d–g), and Caribbean/North Africa (Fig 2h–o). The Ocean category includes trajectories more closely confined to the marine areas to the west of Bermuda. The North America category has trajectories coming from North America, with the case on 17 June having some mixing with North Atlantic air. The ranges of transport times from the coastline of North America to Bermuda for this category were ~ 2–3 d for the MBL and ~ 2 d for the FT. The third category has air masses coming from the southwest in the Caribbean region, with many trajectories derived from North Africa (confirmed with 10 d back-trajectories).

Ocean trajectories are presumed to have more influence from marine-derived emissions such as sea spray and products of marine biogenic emissions of species such as dimethylsulfide (DMS) (Luria et al., 1989; Andreae et al., 2003). North America air masses commonly have more influence from the wide range of anthropogenic sources common to the eastern US, including urban emissions (e.g., vehicular, industrial, combustion), agricultural emissions, and biomass burning (Corral et al., 2021). Finally, the Caribbean/North Africa category is suspected of having more influence from dust, biomass burning, and agricultural emissions, the latter two of which are common around the southeastern US (Sevimoglu and Rogge, 2015; Le Blond et al., 2017; Corral et al., 2020; Edwards et al., 2021; Mardi et al., 2021), as well as the dust derived often from North Africa (Arimoto et al., 1995; Anderson et al., 1996; Todd et al., 2003; Muhs et al., 2012).

Regarding influential weather during the time frame of this study, 5–6 June 2022 was marked by the arrival of Tropical Storm Alex, which transitioned to an extratropical storm and left to the northeast of Bermuda prior to the 7 June flight. Starting on 7 June, a high-pressure system moved into the Bermuda area through 9 June, which was a period marked by the arrival of North America air. After that point, cold fronts moving off the US East Coast shifted the high-pressure system farther east, setting up the classical subtropical Bermuda–Azores High that promotes southwesterly flow into the area, which explains the string of Caribbean/North Africa air mass days between 10 and 14 June. Corresponding to the last spiral on 17 June with North America air, there was another high-pressure system that set up over the Bermuda area.

3.2　Meteorology and trace gases

We next discuss measurements pertaining to basic meteorological variables (Table 3 and Fig. 3) and trace gases (Table 3 and Fig. 4). From the start, we note that, in cases of multiple spirals on the same day, there was no significant change between morning and afternoon measurements of trace gas, meteorological, and aerosol parameters. In situ measurements of temperature show expected reductions from the lowest kilometer (~ 121 °C) to 12–13 °C in the FT between 1 and 3.5 km. While relative humidity decreased too as expected, the reduction for North America air in the FT (1–3.5 km) was more pronounced (relative humidity – RH – ~ 22 %) than for other air mass types (51 %–69 %) when compared to the lowest kilometer (73 %–82 %). Soundings that could reach the highest altitudes in this study show that there were air mass layers aloft (> 5 km), where moisture generally increased for North America and Caribbean/North Africa air masses. Dropsonde profiles were only available for North America and Caribbean/North Africa air masses, and as expected they were consistent with the in situ data of the added feature shown where the dry North American layer extends from ~ 1.8 to 5 km with a moister layer above.
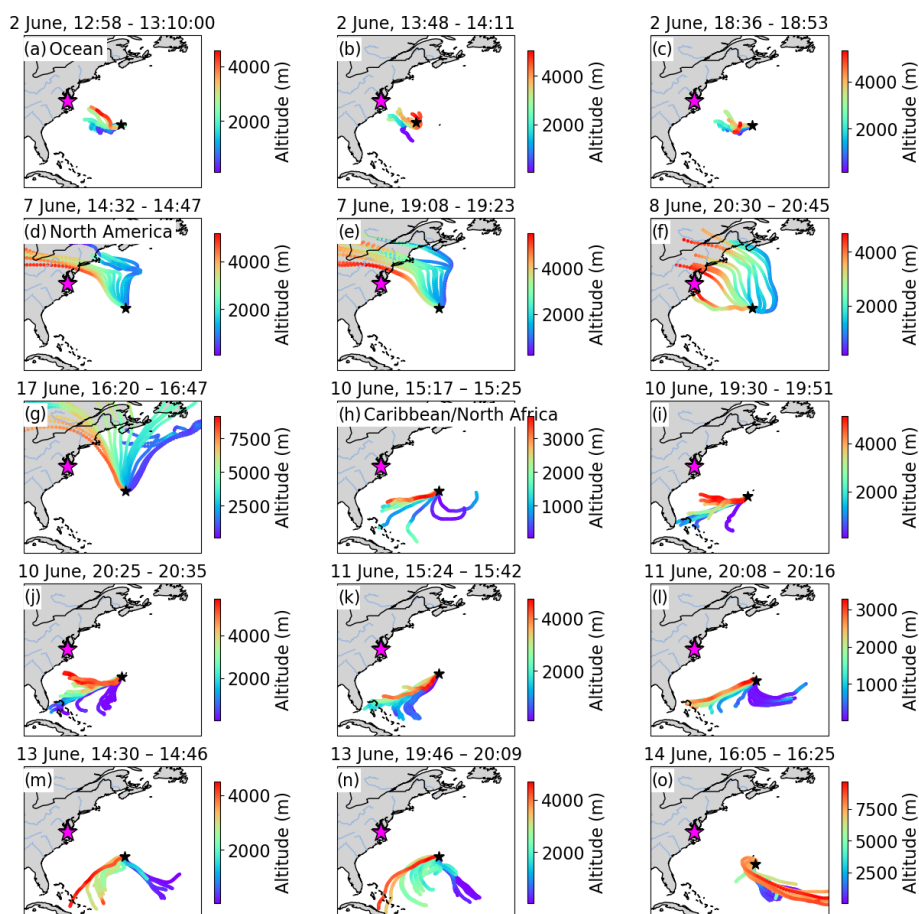
Figure 2. HYSPLIT 3 d back-trajectories ending at the location of the Falcon aircraft at different vertical levels during individual spiral soundings. Panels **(a)**–**(c)** are categorized as Ocean, panels **(d)**–**(g)** as North America, and panels **(h)**–**(o)** as Caribbean/North Africa. The color bar indicates the altitude at each time step of the individual trajectories. The pink and black stars correspond to NASA Langley Research Center (Hampton, Virginia) and Bermuda, respectively. The date and UTC time range of the spirals are above each panel.

While there were sparse data passing quality control criteria for wind speed from the Falcon during the spirals, wind speed data are shown only from dropsondes (only available for North America and Caribbean/North Africa air), revealing wind speeds typically between 5 and 10 m s^{-1}, with more of an increase with altitude for the North America category.

The cumulative amount of precipitation along trajectories up to the point of the Falcon spirals provides a sense of the potential for wet scavenging of particles and soluble gases to occur in transported air masses (Table 3). North America air masses exhibited the highest APT value (19.6 mm) for air sampled in the lowest kilometer during spirals as compared to Ocean (2.2 mm) and Caribbean/North Africa (5.4 mm) air masses (Table 3). The enhanced level for North America air is due to RF178. APT values were generally lower in the 1–3.5 km range as compared to < 1 km.

Carbon dioxide (CO_2) levels were fairly similar at the altitudes examined (Fig. 4), with median values for the altitude bins ranging from ∼ 418 to ∼ 422 ppm. The highest variability at fixed altitude bins, as represented by the whiskers in Fig. 4, was for North America air masses.

We next examine ozone (O_3), which is a critical source of tropospheric OH radicals and is produced by sunlight, volatile organic compounds (VOC), and nitrogen oxides (NO_x), the latter two of which come from a plethora of anthropogenic and natural sources (Cooper et al., 2014). Ozone concentrations generally increased with altitude up to 5 km for all air mass types, with systematically higher (lower) values for North America (Caribbean/North Africa) at a given altitude. The median values (ppbv) in the MBL and FT (1–3.5 km) were 39.60/55.50 (North America), 18.93/43.50 (Ocean), and 14.78/24.20 (Caribbean/North Africa). The maximum ozone value (102.9 ppb) was observed for the North America category at 4.8 km. Elevated O_3 events have been documented previously over Bermuda in the springtime due to presumed downward mixing of air from the stratosphere (Oltmans and Levy, 1992; Moody et al., 1995; Milne et al., 2000), and the results here are consistent with a vertical gradient with enhanced values aloft. One study showed

levels exceeding 100 ppbv from 5 to 15 km above sea level over Bermuda in July 1993 from North America air masses that were 2–5 d old (Merrill et al., 1996). Furthermore, Dickerson et al. (1995) noted that more than half of the air during "ozone episodes", defined as having > 40 ppbv, over Bermuda in June 1992 was due to transport from the boundary layer of eastern North America. For context, Zawadowicz et al. (2021) reported summertime O_3 levels of 10–40 ppbv in the MBL over the eastern North Atlantic, which is consistent with all air mass types except those from North America.

Vertical profiles of CH_4 and CO exhibited varying degrees of variation across the range of altitudes profiled (Table 3). CO is considered a "quasi-conservative" marker for anthropogenic emissions (e.g., fossil fuel and biomass combustion, oxidation of methane and non-methane hydrocarbons) (Fishman and Seiler, 1983; PéTron et al., 2002) with a lifetime of approximately $\sim$ 1–3 months (Holloway et al., 2000). Methane on the other hand has a longer lifetime ($\sim$ 10 years) with diverse sources ranging from soils to fossil fuel combustion (Robson et al., 2018). There was a consistent separation in concentrations at fixed altitudes up to 5 km between the air mass types: North America > Ocean > Caribbean/North Africa. North American CO and CH_4 levels showed the most pronounced reduction with altitude in the lowest 5 km. The vertical structures of the trace gases exhibit relationships with the temperature/relative humidity (T/RH) profiles, suggestive of different air mass layers; this was most distinct for North America air around 1.1 and 5 km and Ocean air around 2 km. Past work over the remote Atlantic such as over the Azores (Honrath et al., 2004) showed that elevated CO and O_3 were attributed to North American pollution outflow and transported smoke plumes from source regions as far as Siberia. Typical CO values in the eastern North Atlantic during summertime were 60–100 ppb (Zawadowicz et al., 2021), which were lower than in winter due to more efficient removal in the summer from oxidation with the OH radical (Logan et al., 1981). Corral et al. (2021) showed that the lowest minimum values across the entire northwestern Atlantic of any season were in the summer over the open ocean by Bermuda. The CO values for North America air masses (> 90 ppb) and to a lesser extent Ocean air masses ($\sim$ 80–90 ppb) over Bermuda tend to be higher than reported background values ($\sim$ 80 ppb) devoid of urban influence (Zuidema et al., 2017; Shilling et al., 2018).

For all four trace gases, Ocean profiles exhibited the lowest variability at fixed altitudes (i.e., the smallest whiskers in Fig. 4), likely due to the three spirals from this category being on the same day without much change across 6 h. FT values of O_3 in the Ocean category show pronounced enhancements relative to MBL values, even approaching O_3 levels from North America air masses, suggesting that FT air in this category is probably influenced by North America emissions. Similarly, Caribbean/North Africa air had a steeply rising O_3 profile up to the highest point shown in Fig. 4 at $\sim$ 8.5 km, which was comparable to North American values.
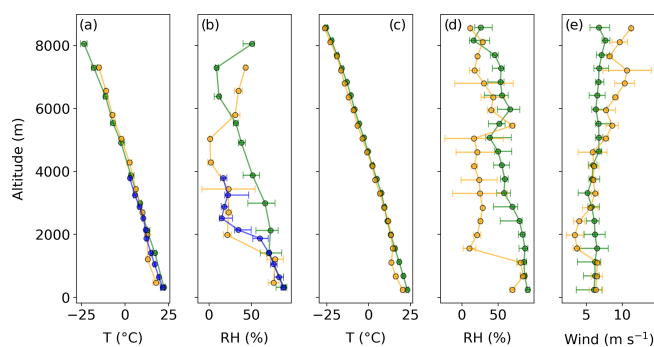
Figure 3. Vertical distribution of meteorological variables as measured (a–b) in situ by the Falcon and (c–e) with dropsondes launched from King Air. Shown are temperature (T), relative humidity (RH), and wind speed (only for King Air) grouped into similar air mass source categories (orange: North America; blue: Ocean; green: Caribbean/North Africa). Markers are the median values, and whiskers are the 25th and 75th percentiles. Data were unavailable for the Ocean category for dropsondes.
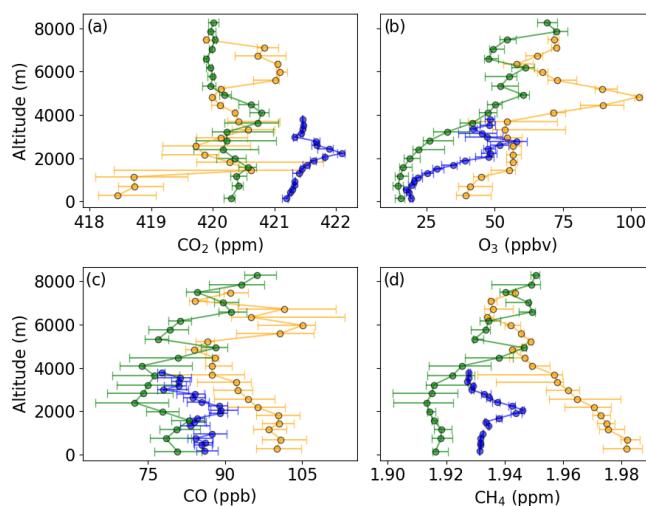
Figure 4. Vertical distribution of trace gas concentrations for each air mass source region (orange: North America; blue: Ocean; green: Caribbean/North Africa). Markers are the median values, and whiskers are the 25th and 75th percentiles. The marine boundary layer heights and aerosol mixing layer heights are shown in Table 1 for reference.

3.3 Particle number and volume concentrations

We next discuss particle number concentration statistics for different size ranges (Fig. 5): 3–10 nm, 10–100 nm, 0.1–1 µm, 1–5 µm, and > 3 µm. Particle concentrations at the smallest sizes (3–10 nm) generally increased with altitude, which is consistent with the literature suggesting that new particle formation in marine regions is more prevalent in the free troposphere (Bianchi et al., 2016; Clarke et al., 1998, 2013; Xiao et al., 2023), due to usually lower aerosol surface areas such as sea salt in particular being a significant sink

Table 3. Median statistics for meteorological and trace gases, as measured by the Falcon aircraft, for three source regions below 1 km and between 1 and 3.5 km. Refer to Figs. 3–4 for the full vertical profiles.

< 1 km	T (°C)	RH (%)	APT (mm)	CH_4 (ppm)	CO_2 (ppm)	CO (ppb)	O_3 (ppbv)
North America	16.98	78.00	19.60	1.98	418.63	100.90	39.60
Ocean	20.03	83.67	2.20	1.93	421.29	86.20	18.93
Caribbean/North Africa	21.11	83.65	5.40	1.92	420.42	80.88	14.78
1–3.5 km							
North America	11.91	24.10	1.10	1.97	420.16	97.85	55.50
Ocean	11.57	44.70	1.35	1.93	421.56	84.80	43.50
Caribbean/North Africa	12.16	76.90	4.90	1.92	420.48	79.67	24.20

for precursor vapors in the MBL. Median number concentrations between 3 and 10 nm in the lowest 1 km and between 1 and 3.5 km ranged between 78–326 and 135–266 cm^{-3}, respectively, for the three air type categories. North America air generally exhibited the highest concentrations at all altitudes, due likely to higher levels of precursor vapors (e.g., NO_x, SO_2, VOCs) from continental outflow (e.g., Corral et al., 2022a). These particles represent an important source of cloud condensation nuclei (CCN) due to their ability to grow to CCN-relevant sizes (e.g., Zheng et al., 2021). The ratio of the number concentration above 3 nm to 10 nm ($N_3 : N_{10}$) is commonly used to infer the influence of new particle formation (NPF) (Corral et al., 2022a, and references therein). This ratio increases with altitude for the full duration of the spiral soundings conducted, ranging from ~ 1.25 at the lowest altitude to ~ 1.8 above 8 km. Table 4 shows that the ratio values were similar amongst the air mass types below 1 km and between 1 and 3.5 km.

Particles in the ranges of 0.01–0.1 and 0.1–1 μm showed comparable number concentrations for the three air categories across the vertical range of measurements, with a general reduction up to approximately 2 km followed by an increase up to higher altitudes. Because the number concentrations of different size ranges within the submicron aerosol population were higher in the FT (especially above 5 km), any air entrained from the FT into the MBL can be an influential source of aerosol and especially CCN around Bermuda. Consistent with most of the trace gases, number concentrations were highest for North America air below a diameter of 1 μm, with the median values (10–100 nm/0.1–1 μm) being 202/297 cm^{-3} for < 1 km and 138/155 cm^{-3} for 1–3.5 km.

While much lower in number concentration than submicron size fraction, supermicron particles are significant owing to their efficient ability to scatter light and influence clouds via effects documented for giant CCN (Houghton, 1938). Figure 5 shows a general reduction in the number of particles with D_p between 1 and 5 μm (from the LAS) and > 3 μm (from the FCDP) with altitude up to approximately 2 km, above which values were negligible; note that the FCDP data are under ambient conditions and are not
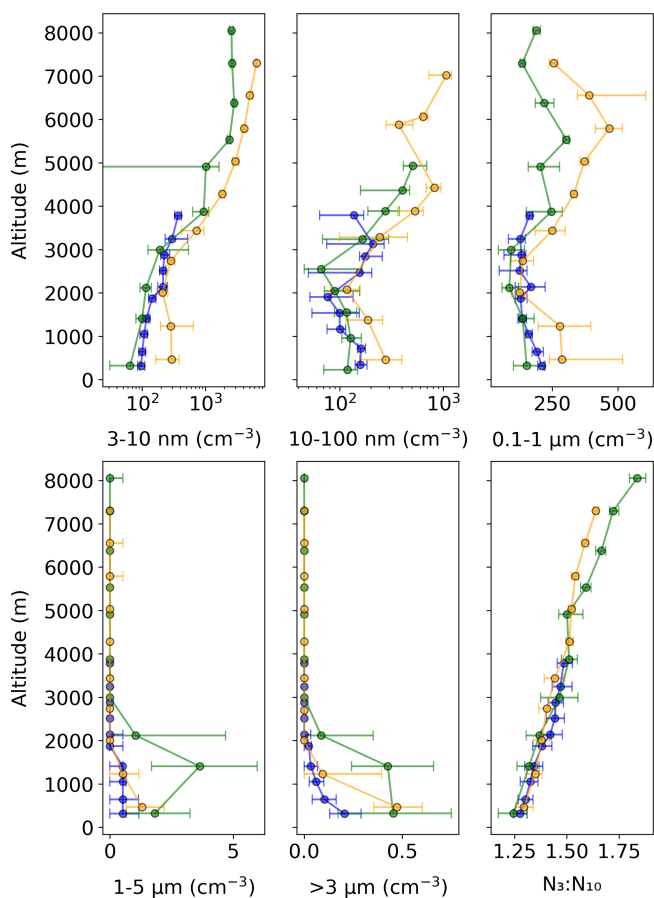
dried like for the LAS. The vertical profiles for supermicron particle concentrations are generally consistent with those reported elsewhere for air masses closer to the US East Coast (Gonzalez et al., 2022) and over Bermuda (Horvath et al., 1990; Kim et al., 1990). Sources of these larger particles will be discussed in the subsequent sections, but the likely candidates are sea salt and dust particles, as expected. The Caribbean/North Africa category exhibited the highest median supermicron number concentrations between 1 and 3.5 km (LAS: 1 cm^{-3}).

Figure S1 and Table S3 in the Supplement show results for aerosol volume concentrations to complement the previous discussion, with the main conclusion that the sub-100 nm volume concentration vertical profiles follow the number concentration in terms of changes with altitude and how North America exhibits the highest values. For 0.1–1, 1–5, and > 3 μm, the highest volume concentration was for the Caribbean/North Africa up to 2 km, without much variation above that level between the categories. These findings contradict previous studies conducted in Bermuda (Horvath et al., 1990; Kim et al., 1990) in that we did not observe a general decrease in both the number and volume concentration from the MBL to the FT. Instead, we observed the highest values for number and volume at higher altitudes, specifically for certain size ranges (i.e., below 1 μm) and types of air masses. It is noted that those earlier studies were limited in terms of the higher altitudes they could report data at, with Kim et al. (1990) and Horvath et al. (1990) reporting FT data at altitudes of 2750 and 1500 m, respectively; additionally, those studies were limited to measurements with wing-mounted optical probes, which introduce additional uncertainties that are well documented in the literature (Porter and Clarke, 1997; Reid et al., 2001, 2006). These comparisons with past work show the importance of the ACTIVATE data for giving a more complete picture of the vertical column above this remote marine location of the northwestern Atlantic. Our results are also consistent with earlier reports of how North American outflow especially can enhance small particle number concentrations in the remote marine atmosphere of the Atlantic (Anderson et al., 1993).

Table 4. Summary of median aerosol number concentration statistics for different diameter size ranges for the three major air mass types. Note that all the diameter ranges are for dry particles, except for $> 3\,\mu m$, which is under ambient RH conditions. The farthest right column is the ratio of the number concentration above 3 nm versus 10 nm and is unitless.

	N (cm^{-3})						
< 1 km	3–10 nm	> 10 nm	10–100 nm	0.1–1 μm	1–5 μm	> 3 μm	$N_3 : N_{10}$
North America	326	1118	202	297	2	0.4	1.30
Ocean	99	334	167	194	1	0.1	1.29
Caribbean/North Africa	78	343	116	146	2	0.4	1.27
1–3.5 km							
North America	266	708	138	155	0	0.0	1.38
Ocean	191	442	99	140	0	0.0	1.41
Caribbean/North Africa	135	461	119	127	1	0.2	1.36

Figure 5. Vertical distribution of aerosol number concentration (MBLHs and MLHs in Table 1 for reference) for flight data grouped into similar air mass source categories (orange: North America; blue: Ocean; green: Caribbean/North Africa). Markers are the median values, and whiskers are the 25th and 75th percentiles. Note that all the diameter ranges are for dry particles, except for $> 3\,\mu m$, which is under ambient RH conditions.

3.4   Lidar retrieval results

The HSRL-2 on the higher-flying King Air provided vertically resolved data for aerosol extinction, which provide additional context for the aerosol vertical structure (Fig. 6). As expected, the vertical profiles follow the aforementioned number and volume concentration results for supermicron particles owing to the sensitivity of light scattering to an aerosol surface area. Extinction values exhibit peaks in the lowest 2 km for the North America and Caribbean/North Africa categories, which is consistent with higher RH and size-resolved particle concentration results. Above 2 km, there is a steep decrease. An exception is a peculiar layer of enhanced extinction around 5–6 km for the North America category due to one particular spiral on 17 June 2022. As shown in Fig. S2 in the Supplement, this was a case of smoke transport from the southwestern US based on HYSPLIT back-trajectory results, a spatial map of smoke over North America from the Navy Aerosol Analysis and Prediction System (NAAPS; https://www.nrlmry.navy.mil/aerosol/, last access: 15 December 2023) (Lynch et al., 2016), and HSRL-2 aerosol type results pertaining to this flight. Figure 4 also shows CO enhancements for North America air around 5–6 km. This highlights the importance of smoke transport during the summer to areas as far offshore of the US as Bermuda, as was alluded to by past work (Mardi et al., 2021). The aerosol extinction vertical distributions are generally consistent with those reported previously over Bermuda by the Cloud-Aerosol Lidar with Orthogonal Polarization (CALIOP) sensor on the Cloud-Aerosol Lidar and Infrared Pathfinder Satellite Observations (CALIPSO) satellite in terms of the influence of sea salt and dust in the summer months (Aldhaif et al., 2021). The Caribbean region had the highest extinction values, reaching as high as $0.17\,km^{-1}$ at an altitude of 0.17 km (RF176 – 14 June 2022). North America's maximum extinction was $0.1\,km^{-1}$ at an altitude of 0.94 km (RF167 – 7 June 2022).

Vertical profiles of the lidar ratio and aerosol depolarization ratio are useful for differentiating between aerosol types

(Burton et al., 2012; Groß et al., 2013). HSRL lidar ratios at 532 nm for Saharan dust tend to be around ~ 45–55 sr (Burton et al., 2012; Groß et al., 2013), whereas values are lower for marine aerosol (< 30 sr) and slightly higher for smoke and urban pollution aerosol ($\sim > 60$ sr); note that the documented ranges can be broader than the values reported here (e.g., Burton et al., 2012; Groß et al., 2013). Values for North America tended to be below 30 sr in the lowest kilometer and in excess of 70 sr above 2 km, which is consistent with the clean marine and polluted continental and smoke categories in the MBL and FT, respectively. The high values above 2 km help support the speculation above that there was a smoke layer contributing to enhanced aerosol extinction at around 5–6 km on 17 June. In contrast, Caribbean/North Africa air had values starting closer to 30 sr in the lowest kilometer and only peaked around ~ 55 sr at 2.5 km, with values closer to 30–35 between 4.38 and 6.17 km, which is more reflective of values associated with Saharan dust aerosol (Burton et al., 2012; Groß et al., 2013). Depolarization ratio values below 0.05 at high RH ($\sim > 65$ % RH) are common for marine aerosols (e.g., Groß et al., 2013; Illingworth et al., 2015; Ferrare et al., 2023), whereas higher values of up to almost 0.25 and 0.28 have been reported for dry sea salt aerosol (Kanngießer and Kahnert, 2021; Ferrare et al., 2023) and dust (Järvinen et al., 2016; Huang et al., 2023), respectively. The results show that, while North America air had depolarization ratios of typically less than 0.1, the Caribbean/North Africa category had values in excess of 0.1 and up to 0.48 at 5.28 km, indicating dust (Burton et al., 2012; Groß et al., 2013), especially since Fig. 3 showed RH values that would rule out dry sea salt.

3.5 Aerosol particle size distribution

Detailed aerosol size distribution data are presented in Fig. 7 using both SMPS and LAS data between 3.16 and 3162 nm using two-mode log-normal curve fitting. Parameter values (number, geometric mean diameter, geometric standard deviation) for both modes are provided in Table 5. Each air mass exhibited two distinct peaks in the BL and FT, notably in the Aitken mode and accumulation mode separated by distinct dips in number consistent with the Hoppel minimum (Hoppel et al., 1986). This suggests that, regardless of the air mass source, the sampled aerosol had probably undergone some cloud processing to transfer constituents from smaller particles in the Aitken mode and gases to larger particles in the accumulation mode. This is consistent with other ACTIVATE measurements conducted around Bermuda during the time of this study with the Falcon (Crosbie et al., 2024). As expected, North America air exhibits a systematically higher number concentration with prominent peaks at diameters of 50/143 and 45/106 nm for < 1 and 1–3.5 km, respectively. For Ocean, the modes were at 63/192 and 35/107 nm for < 1 and 1–3.5 km. Lastly, the Caribbean/North Africa category exhibited modes at 53/177 and 39/92 nm for < 1 and

1–3.5 km, respectively. Thus, there was a decrease in the geometric mean diameter for both modes and all air mass types as a function of altitude from < 1 to 1–3.5 km, suggestive of the air masses not necessarily being related in the MBL and FT.

3.6 Aerosol composition

The next discussion explores AMS submicron composition (Fig. 8 and Table 6), which is relevant to the diameter range between 0.06 and 0.6 µm (Table 2). The total AMS mass concentration was highest for North America across the range of altitudes sampled, with the mean values (μg m^{-3}) below 1 km being 2.66 ± 1.00 (North America), 2.03 ± 0.38 (Ocean), and 1.53 ± 0.52 (Caribbean/North Africa). Values tended to decrease with altitude, with the exception of a notable enhancement between 5 and 7 km (peaking at 2.78 µg m^{-3} as observed at ~ 6500 m) for North America air, which is in line with the enhancement in aerosol volume concentration already shown (Fig. S1) that was attributed to smoke (Fig. S2).

Speciated mass fractions for North America air were distinctly different from the other two categories owing to the dominance of organics, reaching values of 0.49 ± 0.10 and 0.56 ± 0.16 for < 1 and 1–3.5 km, respectively. Sulfate was the next most abundant constituent, followed by ammonium and much lower mass fractions for nitrate and chloride (typically < 0.03). The degree of oxygenation of the organic constituents (f_{44}) was highest for North America air, with mean values of 0.12 ± 0.06 for both altitude ranges in Table 6. These general results for North America air are consistent with past work examining the first 2 years of ACTIVATE flights closer to the US East Coast (Dadashazar et al., 2022), where sulfate and organics dominated the AMS mass concentration but f_{44} values were lower in these Bermuda profiles than the latter study's sample set, which showed values typically between 0.1 and 0.3.

For the Ocean category, sulfate was the most abundant constituent in the lowest 1 km, with a mean mass fraction of 0.64 ± 0.07, followed by ammonium (0.24 ± 0.07) and organics (0.11 ± 0.09). The composition of this category shifted between 1 and 3.5 km to have comparable levels of sulfate and organics with mean mass fractions of 0.38 ± 0.16 and 0.40 ± 0.19, respectively, while that of ammonium was 0.20 ± 0.16.

Lastly, for the Caribbean/North Africa category, the mean mass fractions were similar to those of the Ocean category, with a sulfate-rich profile in the lowest kilometer (mass fraction of 0.65 ± 0.12), which became somewhat more comparable between sulfate and organics between 1 and 3.5 km with mean mass fractions of 0.49 ± 0.54 and 0.37 ± 0.41, respectively. Extending up higher to 8 km, the organic mass fraction for this category kept increasing, with values between 0.5 and 1.0 for various altitude bins between 2 and 6 km.
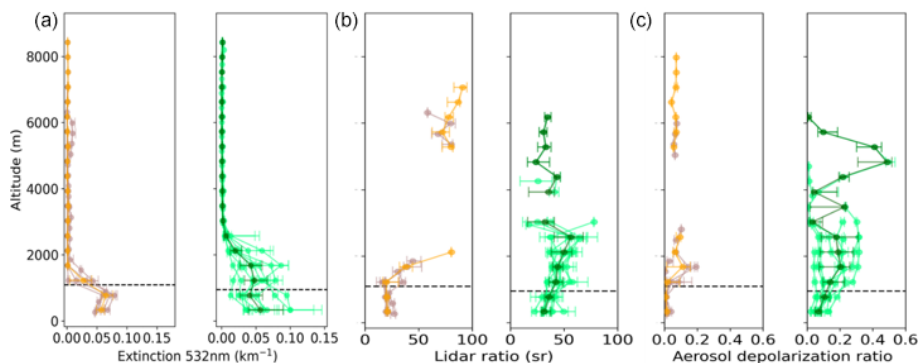
Figure 6. Vertical distribution of the (left) aerosol extinction, (middle) lidar ratio, and (right) aerosol depolarization ratio from HSRL-2 (all at 532 nm) on King Air for the (orange) North America and (green) Caribbean/North Africa air categories. The darker curves represent the median, and the lighter curves represent data from individual overpasses. The dashed horizontal lines represent the mean aerosol MLH, the markers are the median values, and the whiskers are the 25th and 75th percentiles. Missing values indicate unavailable data.
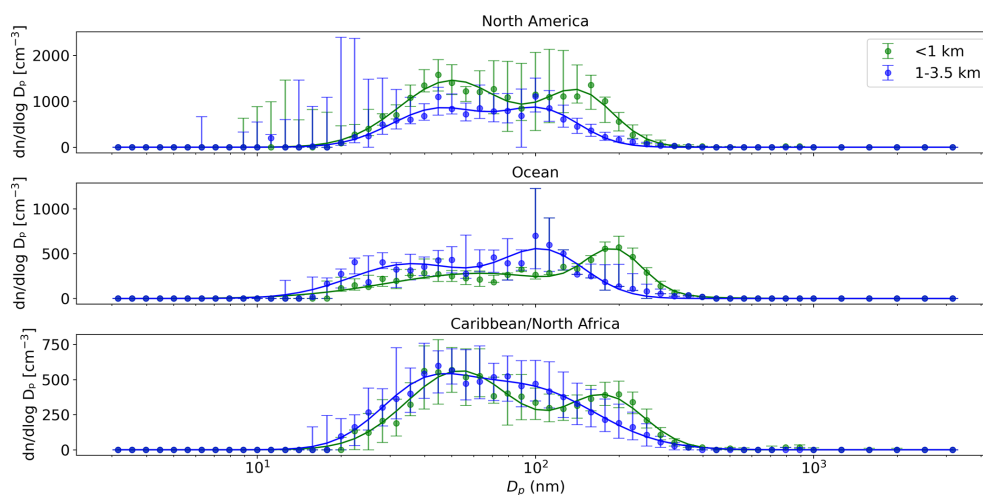
Figure 7. Fitted aerosol number size distributions for data collected during spiral soundings categorized by the three air mass sources. Data are divided into below 1 km and above 1 km. Markers are the median values, and whiskers are the 25th and 75th percentiles.

Table 7 summarizes the water-soluble composition results from the PILS, which offers insight into species not measured by the AMS and a look at a broader size range up to 5 μm. PILS data were combined for entire spiral soundings without separation into altitude layers owing to the lengthier time resolution to obtain samples as compared to the other instrument datasets. When viewing total mass as the sum of concentrations ($\mu g\,m^{-3}$) of the species shown (using total sulfate rather than nss sulfate for calculation of the total mass), North America exhibited the highest mean value (13.26 ± 6.47), followed by Caribbean/North Africa (5.18 ± 3.26) and Ocean (3.65 ± 2.27). The stretch of three flights between 7 and 8 June for North America air was noteworthy, where the total masses were significantly higher than for other flights (up to $20.03\,\mu g\,m^{-3}$ for RF166), which we attribute to the weather conditions associated with the passage of Tropical Storm Alex where high winds could have

helped promote more sea salt emissions. This is confirmed by the high Na^+ and Cl^- mass fractions for those particular flights (0.29–0.55 for Na^+, 0.32–0.47 for Cl^-). The high APT values associated with RF178 do not translate to significantly lower PILS mass concentrations as compared to other flights: RF178 had the second highest total PILS mass ($12.91\,\mu g\,m^{-3}$) due to high Na^+ and Cl^- contributions from sea salt. As it relates to APT, the mean value for each spiral showed no significant relationship with either AMS or PILS total mass or with the total volume concentration between 0.01 and 5 μm from the LAS (Fig. S3). Past work for surface aerosol over Bermuda showed that the winter season is characterized by the most wet scavenging as compared to other seasons in terms of air masses arriving at Bermuda from distant continents (Dadashazar et al., 2021). Aside from the limitations of relying on APT as a metric for wet scavenging of aerosol, a lack of any relationship with APT (Fig. S3) also

Table 5. Two-mode lognormal model parameters for spirals categorized by source region. N: total number concentration; D_g: geometric mean diameter; σ_g: geometric standard deviation.

< 1 km	N_1 (cm^{-3})	$D_{g,1}$ (nm)	$\sigma_{g,1}$	N_2 (cm^{-3})	$D_{g,2}$ (nm)	$\sigma_{g,1}$
North America	1594	50	1.54	855	143	1.34
Ocean	538	63	2.15	274	192	1.27
Caribbean/North Africa	620	53	1.55	312	177	1.39
1–3.5 km						
North America	829	45	1.48	613	106	1.37
Ocean	473	36	1.63	455	107	1.41
Caribbean/North Africa	345	39	1.45	627	92	1.76
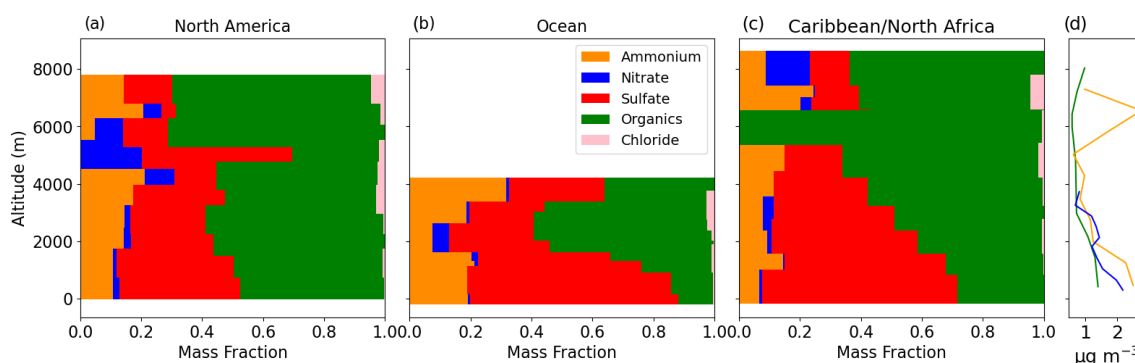
Figure 8. Vertical distribution of AMS **(a–c)** speciated mass fractions (red: sulfate; green: organics; blue: nitrate; orange: ammonium; pink: chloride) and **(d)** total mass concentrations for each air mass type (orange: North America; blue: Ocean; green: Caribbean/North Africa).

builds on findings that precipitation may actually be a source of particles rather than just a sink (e.g., Khadir et al., 2023).

The unique feature of the Caribbean/North Africa spirals was the higher mass fraction for Ca^{2+}, especially on RF174 (0.31), which suggests the presence of dust and which is consistent with the results shown already for how supermicron particles were enhanced for this air mass type (e.g., Figs. 5–6 and S1) for particles larger than 1 µm.

We assessed the potential for sea salt reactivity in the form of chloride depletion by comparing the mass ratio $Cl^- : Na^+$ between different spiral soundings, with a value of 1.8 being attributed to pure sea salt. The mean $Cl^- : Na^+$ ratios for the three air mass types were 0.70 ± 0.40 (Ocean), 1.39 ± 0.37 (North America), and 1.40 ± 0.69 (Caribbean/North Africa). While the Ocean spirals exhibited the lowest overall mass concentrations, they did have the highest relative combined amount of nitrate, nss sulfate, and oxalate, which are key acidic species participating in chloride depletion. The results suggest that the sea salt sampled, regardless of the air mass origin, had potentially experienced a loss of chloride due to reactions with acidic species. We note though that the use of the $Cl^- : Na^+$ ratio to assess chloride depletion has limitations owing to the assumption that sea salt is the only source of the two species used in the ratio, which becomes a challenge for the Caribbean/North Africa category at least,

where there is evidence supporting the presence of dust. The reader is referred elsewhere for a more detailed discussion of sea salt reactivity during ACTIVATE and over Bermuda (Edwards et al., 2023).

To put the aerosol composition results into perspective, measurements in June at the Pico Mountain Observatory in the Azores (i.e., a free tropospheric site representative of transported North America air) revealed aging exceeding 10 d, with the most abundant aerosol types being carbonaceous, followed by sea salt with sulfate (Cheng et al., 2022). Another study at the same site reported evidence of both North American wildfire emissions and continental outflow, with the latter having more oxidized organics (O : C ratio of 0.57), even though it had 3 d transport time from the continent versus 7–10 d for the smoke plumes that exhibited O : C ratios of around 0.45–0.48 (Schum et al., 2018). Measurements in the MBL of the Azores during the Aerosol and Cloud Experiment in the Eastern North Atlantic (ACE-ENA) campaign revealed average AMS mass loadings of 0.6 µg m^{-3} in summer, with sulfate dominating (69 %), followed by organics (23 %), ammonium (23 %), and nitrate (1 %) (Zawadowicz et al., 2021). They also found that North American biomass burning reaching the site enhanced aerosol levels in the FT, along with the background CCN budget being heavily influenced by sulfate from ocean

Table 6. Mean statistics for the AMS speciated mass fraction and total concentration, along with the f_{44} ratio, for the three air mass source regions below and above 1 km. Also shown are mean $f(RH)$ values on the far right.

< 1 km	Organics	SO$_4$	NO$_3$	NH$_4$	Cl	f_{44}	Total AMS mass ($\mu g \, m^{-3}$)	$f(RH)$
North America	0.49	0.39	0.02	0.10	0.00	0.12	2.66	1.38
Ocean	0.11	0.64	< 0	0.24	0.01	< 0	2.03	1.48
Caribbean/North Africa	0.19	0.65	0.01	0.16	0.00	< 0	1.53	0.95
1–3.5 km								
North America	0.56	0.28	0.01	0.15	0.01	0.12	1.41	1.38
Ocean	0.40	0.38	0.02	0.20	0.01	0.04	1.20	1.22
Caribbean/North Africa	0.37	0.49	< 0	0.15	< 0	0.05	0.99	0.88

biogenic emissions. Thus, our results are consistent with the types of air masses sampled (e.g., North American outflow, including smoke) and sulfate being more influential in the MBL than the FT, where organics were relatively more important.

3.7 Aerosol hygroscopicity

Figure 9a and Table 6 present vertically resolved results for submicron $f(RH)$, which is an indicator of subsaturated hygroscopicity as it compares light scattering of particles at RHs of 80 % to 20 %. The $f(RH)$ values were highest for the North America and Ocean categories. The mean values for North America and Ocean for < 1 and 1–3.5 km were 1.38/1.48 and 1.38/1.22, respectively. The Caribbean/North Africa category exhibited lower $f(RH)$ values for < 1 km (0.95) and 1–3.5 km (0.88). Typically, $f(RH)$ values are ≥ 1, especially for urban and marine-derived particles (e.g., Shingler et al., 2016a), but it is not uncommon to have values below 1, suggesting that particles are optically smaller after humidification (e.g., Shingler et al., 2016b). Forthcoming work will aim to examine $f(RH)$ more deeply across all ACTIVATE flights and to probe the values below unity more deeply, which can have a range of explanations.

The key driver of hygroscopicity is aerosol chemical composition. Dadashazar et al. (2022) examined the first 2 years of ACTIVATE data (2020–2021) for Falcon flights closer to the US East Coast and showed that the $f(RH)$ values for "below cloud base (BCB)" legs were inversely related to the organic mass fraction (MF$_{org}$). More specifically, they extrapolated best-fit lines comparing $f(RH)$ to organic mass fraction to show that the characteristic $f(RH)$ values for pure inorganic (i.e., MF$_{org} = 0$) and organic (i.e., MF$_{org} = 1$) aerosol were 1.39 and 1.22, respectively. Figure 9b–d illustrate the relationship between $f(RH)$ and organic mass fraction for the three air mass types, with an inverse relationship observed for the North America and Ocean categories. These two categories varied in terms of their scatterplots due to more data being available for the lowest MF$_{org}$ values (< 0.25) for Ocean, in contrast to more data being available

for the highest MF$_{org}$ values (> 0.75) for North America. The Caribbean/North Africa category had data across the full spectrum of MF$_{org}$, and its lack of an inverse relationship appears to be due to reduced $f(RH)$ values at the lowest MF$_{org}$ values. This may be due to species undetected by the AMS, such as dust and other potential absorbing aerosol types that are non-hygroscopic; we note that the $f(RH)$ data are for submicron aerosol, but there can still be non-hygroscopic aerosol types such as dust in that diameter range. This is consistent with past surface-based measurements at Tudor Hill in Bermuda (Moody et al., 2014) showing that air masses from North Africa exhibited pronounced levels of larger absorbing aerosol types (mainly dust) that are typically less hygroscopic (e.g., Denjean et al., 2015; Kandler et al., 2018; Edwards et al., 2021) as compared to combustion-derived particle types originating from North America. Similar to Dadashazar et al. (2022), we computed $f(RH)$ for the extremes of MF$_{org}$ for the two air categories suspected of being much less affected by refractory species undetected by the AMS (North America/Ocean): pure inorganic = 1.58/1.54 and pure organic = 1.07/0.85. One hypothesis for the higher pure inorganic values here as compared to the study of Dadashazar et al. (2022) is that these data are farther offshore, where there is less influence from carbonaceous components and more relative influence from inorganic species such as sulfate and sea salt; future work will examine composition–hygroscopicity relationships in greater detail for the ACTIVATE dataset.

4 Conclusions

A total of 15 vertical spiral soundings conducted by a HU-25 Falcon over Bermuda from 2 to 17 June 2022 were categorized into three air mass sources to provide insights into trace gas and aerosol characteristics. This is motivated by a large inventory of past studies (Table S1) that examined these and related topics but did not have a large extent of vertically resolved information, which is a gap addressed by this study. An important result in this work is that the vertical characteristics of this remote marine region depend on air mass origin

Table 7. Mass fraction and total mass of water-soluble aerosol chemical composition (PILS) for the 15 spirals categorized by air mass source region. The mean values for each air mass category are shown in the bottom three rows.

Research flight date (mm/dd/yyyy)	Total mass ($\mu g\,m^{-3}$)	Na^+	K^+	Mg^{2+}	Ca^{2+}	Cl^-	NO_3^-	SO_4^{2-}	NSS SO_4^{2-}	Oxalate	$Cl^-:Na^+$	Air mass category
162 – 06/02/2022	2.00	0.17	0.01	0.03	0.04	0.15	0.26	0.35	0.31	0.00	0.89	Ocean
162 – 06/02/2022	5.24	0.21	0.01	0.02	0.02	0.19	0.22	0.32	0.27	0.00	0.93	Ocean
163 – 06/02/2022	2.09	0.40	0.02	0.04	0.03	0.06	0.16	0.28	0.18	0.01	0.27	Ocean
166 - 06/07/2022	20.03	0.29	0.01	0.02	0.01	0.45	0.10	0.11	0.04	0.00	1.55	North America
167 – 06/07/2022	7.72	0.55	0.01	0.04	0.00	0.32	0.03	0.05	0	0.00	0.59	North America
168 – 06/08/2022	9.63	0.32	0.01	0.02	0.02	0.47	0.04	0.12	0.04	0.00	1.47	North America
169 – 06/10/2022	7.53	0.26	0.00	0.01	0.01	0.42	0.09	0.21	0.14	0.00	1.63	Caribbean/North Africa
169 – 06/10/2022	3.70	0.36	0.01	0.03	0.03	0.15	0.17	0.23	0.14	0.00	0.61	Caribbean/North Africa
170 – 06/10/2022	7.47	0.20	0.02	0.03	0.01	0.30	0.18	0.27	0.22	0.01	1.52	Caribbean/North Africa
171 – 06/11/2022	3.26	0.22	0.02	0.03	0.07	0.19	0.23	0.24	0.19	0.00	0.85	Caribbean/North Africa
172 – 06/11/2022	5.64	0.10	0.02	0.06	0.07	0.13	0.29	0.28	0.25	0.05	2.18	Caribbean/North Africa
173 – 06/13/2022	5.31	0.20	0.01	0.03	0.02	0.29	0.18	0.27	0.22	0.01	1.45	Caribbean/North Africa
174 – 06/13/2022	3.15	0.08	0.05	0.04	0.31	0.13	0.16	0.23	0.21	0.01	1.50	Caribbean/North Africa
176 – 06/14/2022	3.86	0.15	0.01	0.02	0.03	0.20	0.27	0.31	0.27	0.00	1.29	Caribbean/North Africa
178 – 06/17/2022	12.91	0.28	0.01	0.03	0.00	0.43	0.12	0.13	0.06	0.00	1.54	North America
Air mass category												
North America	13.26	0.33	0.01	0.03	0.01	0.43	0.08	0.11	0.05	0.00	1.39	
Ocean	3.65	0.27	0.02	0.03	0.03	0.14	0.20	0.32	0.25	0.00	0.70	
Caribbean/North Africa	5.18	0.20	0.02	0.03	0.06	0.22	0.20	0.26	0.21	0.01	1.40	
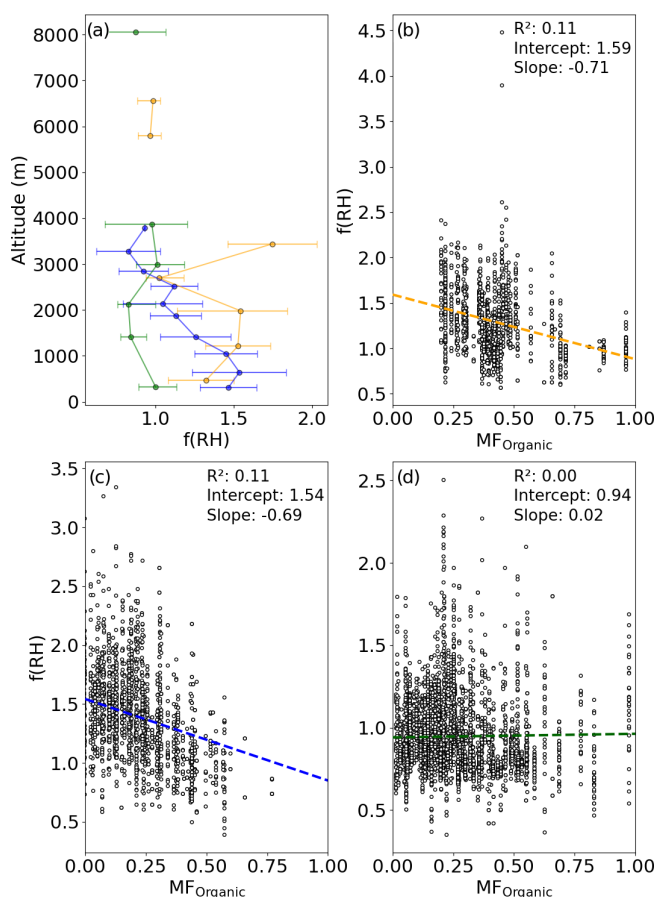
Figure 9. (a) Vertical distribution of f(RH) values (markers: median; whiskers: 25th and 75th percentiles), along with **(b–d)** scatterplots of f(RH) versus the AMS organic mass fraction for the three air mass source regions (**b** North America; **c** Ocean; **d** Caribbean/North Africa).

and that there is significant vertical variability in most trace gas and aerosol variables examined for a given air mass type. The latter point is important in terms of putting into perspective the limitations of column- and surface-based measurements, which have been archived for this (e.g., Aryal et al., 2014) and other remote marine regions.

Trace gases show considerable layering with altitude, with O_3 showing the most pronounced increase with altitude up to ~ 8 km and a peak value of 102.9 ppb at 4.8 km for the North America air mass category. Particle concentrations exhibit altitude-dependent variations, with new particle formation and higher submicron number concentrations more prevalent in the FT, in contrast to higher supermicron number concentrations in the MBL. In contrast to previous studies in Bermuda, we did not observe a general decrease in both number and volume concentrations when ascending from the MBL to the FT, which is presumed to be due to limitations in past works in terms of the altitude range examined in the FT. Analyses of aerosol size distribution data reveal clear peaks

in the Aitken and accumulation modes, which is suggestive of the influence of cloud processing. AMS aerosol composition results show that organics dominate in North America air, whereas Ocean and Caribbean/North Africa air masses had a higher sulfate mass fraction. While sea salt and sulfate were relatively more important in the MBL, organics are relatively more influential in the FT along with dust when trajectories come along the Caribbean/North Africa pathway. Aerosols from the North America and Ocean regions had greater f(RH) values than those from the Caribbean/North Africa region, with a stronger dependence on the organic mass fraction (inverse relationship) for the former two categories.

It is important to consider some limitations in this study to improve upon in future work, such as a need for more statistics (e.g., limited data here for the Ocean category), a need for more detailed gas-phase measurements (e.g., SO_2, DMS, volatile organic compounds), a lack of measurements relating to supermicron particle impacts on aerosol optical properties, and the difficulty of having low-time-resolution measurements (e.g., PILS) for vertical profiles. This work motivates continued attention to the vertical inhomogeneity of trace gas and aerosol properties over remote marine regions and provides a special database to help surface-based data over Bermuda, where atmospheric research has been a rich field for several decades (Sorooshian et al., 2020).

References

ACTIVATE Science Team: Aerosol Cloud meTeorology Interactions oVer the western ATlantic Experiment Data, NASA [data set], https://doi.org/10.5067/SUBORBITAL/ACTIVATE/DATA001, 2020.

Aldhaif, A. M., Stahl, C., Braun, R. A., Moghaddam, M. A., Shingler, T., Crosbie, E., Sawamura, P., Dadashazar, H., Ziemba, L., Jimenez, J. L., Campuzano-Jost, P., and Sorooshian, A.: Characterization of the Real Part of Dry Aerosol Refractive Index Over North America From the Surface to 12 km, J. Geophys. Res.-Atmos., 123, 8283–8300, https://doi.org/10.1029/2018JD028504, 2018.

Aldhaif, A. M., Lopez, D. H., Dadashazar, H., Painemal, D., Peters, A. J., and Sorooshian, A.: An Aerosol Climatology and Implications for Clouds at a Remote Marine Site: Case Study Over Bermuda, J. Geophys. Res.-Atmos., 126, e2020JD034038, https://doi.org/10.1029/2020JD034038, 2021.

Anderson, B. E., Gregory, G. L., Barrick, J. D. W., Collins Jr., J. E., Sachse, G. W., Bagwell, D., Shipham, M. C., Bradshaw, J. D., and Sandholm, S. T.: The impact of U.S. continental outflow on ozone and aerosol distributions over the western Atlantic, J. Geophys. Res.-Atmos., 98, 23477–23489, https://doi.org/10.1029/93JD01208, 1993.

Anderson, J. R., Buseck, P. R., Patterson, T. L., and Arimoto, R.: Characterization of the Bermuda tropospheric aerosol by combined individual-particle and bulk-aerosol analysis, Atmos. Environ., 30, 319–338, https://doi.org/10.1016/1352-2310(95)00170-4, 1996.

Andreae, M. O., Andreae, T. W., Meyerdierks, D., and Thiel, C.: Marine sulfur cycling and the atmospheric aerosol over the springtime North Atlantic, Chemosphere, 52, 1321–1343, https://doi.org/10.1016/S0045-6535(03)00366-7, 2003.

Arimoto, R., Duce, R. A., Ray, B. J., Ellis Jr., W. G., Cullen, J. D., and Merrill, J. T.: Trace elements in the atmosphere over the North Atlantic, J. Geophys. Res.-Atmos., 100, 1199–1213, https://doi.org/10.1029/94JD02618, 1995.

Arimoto, R., Duce, R. A., Ray, B. J., and Tomza, U.: Dry deposition of trace elements to the western North Atlantic, Global Biogeochem. Cy., 17, 1010, https://doi.org/10.1029/2001GB001406, 2003.

Aryal, R. P., Voss, K. J., Terman, P. A., Keene, W. C., Moody, J. L., Welton, E. J., and Holben, B. N.: Comparison of surface and column measurements of aerosol scattering properties over the western North Atlantic Ocean at Bermuda, Atmos. Chem. Phys., 14, 7617–7629, https://doi.org/10.5194/acp-14-7617-2014, 2014.

Bianchi, F., Tröstl, J., Junninen, H., Frege, C., Henne, S., Hoyle, C. R., Molteni, U., Herrmann, E., Adamov, A., Bukowiecki, N., Chen, X., Duplissy, J., Gysel, M., Hutterli, M., Kangasluoma, J., Kontkanen, J., Kürten, A., Manninen, H. E., Münch, S., Peräkylä, O., Petäjä, T., Rondo, L., Williamson, C., Weingartner, E., Curtius, J., Worsnop, D. R., Kulmala, M., Dommen, J., and Baltensperger, U.: New particle formation in the free troposphere: A question of chemistry and timing, Science, 352, 1109–1112, https://doi.org/10.1126/science.aad5456, 2016.

Burton, S. P., Ferrare, R. A., Hostetler, C. A., Hair, J. W., Rogers, R. R., Obland, M. D., Butler, C. F., Cook, A. L., Harper, D. B., and Froyd, K. D.: Aerosol classification using airborne High Spectral Resolution Lidar measurements – methodology and examples, Atmos. Meas. Tech., 5, 73–98, https://doi.org/10.5194/amt-5-73-2012, 2012.

Burton, S. P., Hair, J. W., Kahnert, M., Ferrare, R. A., Hostetler, C. A., Cook, A. L., Harper, D. B., Berkoff, T. A., Seaman, S. T., Collins, J. E., Fenn, M. A., and Rogers, R. R.: Observations of the spectral dependence of linear particle depolarization ratio of aerosols using NASA Langley airborne High Spectral Resolution Lidar, Atmos. Chem. Phys., 15, 13453–13473, https://doi.org/10.5194/acp-15-13453-2015, 2015.

Burton, S. P., Hostetler, C. A., Cook, A. L., Hair, J. W., Seaman, S. T., Scola, S., Harper, D. B., Smith, J. A., Fenn, M. A., Ferrare, R. A., Saide, P. E., Chemyakin, E. V., and Müller, D.: Calibration of a high spectral resolution lidar using a Michelson interferometer, with data examples from ORACLES, Appl. Opt., 57, 6061–6075, https://doi.org/10.1364/AO.57.006061, 2018.

Cheng, Z., Morgenstern, M., Zhang, B., Fraund, M., Lata, N. N., Brimberry, R., Marcus, M. A., Mazzoleni, L., Fialho, P., Henning, S., Wehner, B., Mazzoleni, C., and China, S.: Particle phase-state variability in the North Atlantic free troposphere during summertime is determined by atmospheric transport patterns and sources, Atmos. Chem. Phys., 22, 9033–9057, https://doi.org/10.5194/acp-22-9033-2022, 2022.

Clarke, A. D., Varner, J. L., Eisele, F., Mauldin, R. L., Tanner, D., and Litchy, M.: Particle production in the remote marine atmosphere: Cloud outflow and subsidence during ACE 1, J. Geophys. Res.-Atmos., 103, 16397–16409, https://doi.org/10.1029/97JD02987, 1998.

Clarke, A. D., Freitag, S., Simpson, R. M. C., Hudson, J. G., Howell, S. G., Brekhovskikh, V. L., Campos, T., Kapustin, V. N., and Zhou, J.: Free troposphere as a major source of CCN for the equatorial pacific boundary layer: long-range transport and teleconnections, Atmos. Chem. Phys., 13, 7511–7529, https://doi.org/10.5194/acp-13-7511-2013, 2013.

Cooper, O. R., Parrish, D. D., Ziemke, J., Balashov, N. V., Cupeiro, M., Galbally, I. E., Gilge, S., Horowitz, L., Jensen, N. R., Lamarque, J.-F., Naik, V., Oltmans, S. J., Schwab, J., Shindell, D. T., Thompson, A. M., Thouret, V., Wang, Y., and Zbinden, R. M.: Global distribution and trends of tropospheric ozone: An observation-based review, Elementa, 2, 000029, https://doi.org/10.12952/journal.elementa.000029, 2014.

Corral, A. F., Dadashazar, H., Stahl, C., Edwards, E.-L., Zuidema, P., and Sorooshian, A.: Source Apportionment of Aerosol at a Coastal Site and Relationships with Precipitation Chemistry: A Case Study over the Southeast United States, Atmosphere, 11, 1212, https://doi.org/10.3390/atmos11111212, 2020.

Corral, A. F., Braun, R. A., Cairns, B., Gorooh, V. A., Liu, H., Ma, L., Mardi, A. H., Painemal, D., Stamnes, S., van Diedenhoven, B., Wang, H., Yang, Y., Zhang, B., and Sorooshian, A.: An Overview of Atmospheric Features Over the Western North Atlantic Ocean and North American East Coast – Part 1: Analysis of Aerosols, Gases, and Wet Deposition Chemistry, J. Geophys. Res.-Atmos., 126, e2020JD032592, https://doi.org/10.1029/2020jd032592, 2021.

Corral, A. F., Choi, Y., Crosbie, E., Dadashazar, H., DiGangi, J. P., Diskin, G. S., Fenn, M., Harper, D. B., Kirschler, S., Liu, H., Moore, R. H., Nowak, J. B., Scarino, A. J., Seaman, S., Shingler, T., Shook, M. A., Thornhill, K. L., Voigt, C., Zhang, B., Ziemba, L. D., and Sorooshian, A.: Cold Air Outbreaks Promote New Particle Formation Off the U.S. East Coast, Geophys. Res. Lett., 49, e2021GL096073, https://doi.org/10.1029/2021GL096073, 2022a.

Corral, A. F., Choi, Y., Collister, B. L., Crosbie, E., Dadashazar, H., DiGangi, J. P., Diskin, G. S., Fenn, M., Kirschler, S., Moore, R. H., Nowak, J. B., Shook, M. A., Stahl, C. T., Shingler, T., Thornhill, K. L., Voigt, C., Ziemba, L. D., and Sorooshian, A.: Dimethylamine in cloud water: a case study over the northwest Atlantic Ocean, Environ. Sci.-Atmos., 2, 1534–1550, https://doi.org/10.1039/D2EA00117A, 2022b.

Crosbie, E., Ziemba, L. D., Shook, M. A., Robinson, C. E., Winstead, E. L., Thornhill, K. L., Braun, R. A., MacDonald, A. B., Stahl, C., Sorooshian, A., Van Den Heever, S. C., DiGangi, J. P., Diskin, G. S., Woods, S., Bañaga, P., Brown, M. D., Gallo, F., Hilario, M. R. A., Jordan, C. E., Leung, G. R., Moore, R. H., Sanchez, K. J., Shingler, T. J., and Wiggins, E. B.: Measurement report: Closure analysis of aerosol–cloud composition in tropical maritime warm convection, Atmos. Chem. Phys., 22, 13269–13302, https://doi.org/10.5194/acp-22-13269-2022, 2022.

Crosbie, E., Ziemba, L., Shook, M., Shingler, T., Hair, J., Sorooshian, A., Ferrare, R., Cairns, B., Choi, Y., DiGangi, J., Diskin, G., Hostetler, C., Kirschler, S., Moore, R. H., Painemal, D., Robinson, C., Seaman, S., Thornhill, K., Voigt,

C., and Winstead, E.: Measurement Report: Cloud and environmental properties associated with aggregated shallow marine cumulus and cumulus congestus, EGUsphere [preprint], https://doi.org/10.5194/egusphere-2024-148, 2024.

Dadashazar, H., Alipanah, M., Hilario, M. R. A., Crosbie, E., Kirschler, S., Liu, H., Moore, R. H., Peters, A. J., Scarino, A. J., Shook, M., Thornhill, K. L., Voigt, C., Wang, H., Winstead, E., Zhang, B., Ziemba, L., and Sorooshian, A.: Aerosol responses to precipitation along North American air trajectories arriving at Bermuda, Atmos. Chem. Phys., 21, 16121–16141, https://doi.org/10.5194/acp-21-16121-2021, 2021.

Dadashazar, H., Corral, A. F., Crosbie, E., Dmitrovic, S., Kirschler, S., McCauley, K., Moore, R., Robinson, C., Schlosser, J. S., Shook, M., Thornhill, K. L., Voigt, C., Winstead, E., Ziemba, L., and Sorooshian, A.: Organic enrichment in droplet residual particles relative to out of cloud over the northwestern Atlantic: analysis of airborne ACTIVATE data, Atmos. Chem. Phys., 22, 13897–13913, https://doi.org/10.5194/acp-22-13897-2022, 2022.

DeCarlo, P. F., Kimmel, J. R., Trimborn, A., Northway, M. J., Jayne, J. T., Aiken, A. C., Gonin, M., Fuhrer, K., Horvath, T., Docherty, K. S., Worsnop, D. R., and Jimenez, J. L.: Field-Deployable, High-Resolution, Time-of-Flight Aerosol Mass Spectrometer, Anal. Chem., 78, 8281–8289, https://doi.org/10.1021/ac061249n, 2006.

Denjean, C., Caquineau, S., Desboeufs, K., Laurent, B., Maille, M., Quiñones Rosado, M., Vallejo, P., Mayol-Bracero, O. L., and Formenti, P.: Long-range transport across the Atlantic in summertime does not enhance the hygroscopicity of African mineral dust, Geophys. Res. Lett., 42, 7835–7843, https://doi.org/10.1002/2015GL065693, 2015.

Dickerson, R. R., Doddridge, B. G., Kelley, P., and Rhoads, K. P.: Large-scale pollution of the atmosphere over the remote Atlantic Ocean: Evidence from Bermuda, J. Geophys. Res.-Atmos., 100, 8945–8952, https://doi.org/10.1029/95JD00073, 1995.

DiGangi, J. P., Choi, Y., Nowak, J. B., Halliday, H. S., Diskin, G. S., Feng, S., Barkley, Z. R., Lauvaux, T., Pal, S., Davis, K. J., Baier, B. C., and Sweeney, C.: Seasonal Variability in Local Carbon Dioxide Biomass Burning Sources Over Central and Eastern US Using Airborne In Situ Enhancement Ratios, J. Geophys. Res.-Atmos., 126, e2020JD034525, https://doi.org/10.1029/2020JD034525, 2021.

Diskin, G. S., Podolske, J. R., Sachse, G. W., and Slate, T. A.: Open-path airborne tunable diode laser hygrometer, in: Diode Lasers and Applications in Atmospheric Sensing, P. Soc. Photo.-Opt. Ins., 4817, 196–204, https://doi.org/10.1117/12.453736, 2002.

Easter, R. C., Ghan, S. J., Zhang, Y., Saylor, R. D., Chapman, E. G., Laulainen, N. S., Abdul-Razzak, H., Leung, L. R., Bian, X., and Zaveri, R. A.: MIRAGE: Model description and evaluation of aerosols and trace gases, J. Geophys. Res.-Atmos., 109, D20, https://doi.org/10.1029/2004JD004571, 2004.

Edwards, E.-L., Corral, A. F., Dadashazar, H., Barkley, A. E., Gaston, C. J., Zuidema, P., and Sorooshian, A.: Impact of various air mass types on cloud condensation nuclei concentrations along coastal southeast Florida, Atmos. Environ., 254, 118371, https://doi.org/10.1016/j.atmosenv.2021.118371, 2021.

Edwards, E.-L., Reid, J. S., Xian, P., Burton, S. P., Cook, A. L., Crosbie, E. C., Fenn, M. A., Ferrare, R. A., Freeman, S. W., Hair, J. W., Harper, D. B., Hostetler, C. A., Robinson, C. E., Scarino,

A. J., Shook, M. A., Sokolowsky, G. A., van den Heever, S. C., Winstead, E. L., Woods, S., Ziemba, L. D., and Sorooshian, A.: Assessment of NAAPS-RA performance in Maritime Southeast Asia during CAMP²Ex, Atmos. Chem. Phys., 22, 12961–12983, https://doi.org/10.5194/acp-22-12961-2022, 2022.

Edwards, E.-L., Choi, Y., Crosbie, E. C., DiGangi, J. P., Diskin, G. S., Robinson, C. E., Shook, M. A., Winstead, E. L., Ziemba, L. D., and Sorooshian, A.: Sea salt reactivity over the northwest Atlantic: An in-depth look using the airborne ACTIVATE dataset, EGUsphere [preprint], https://doi.org/10.5194/egusphere-2023-2575, 2023.

Fernandes, A., Szkop, A., and Pietruczuk, A.: Comparison of the Performance of the GRASP and MERRA2 Models in Reproducing Tropospheric Aerosol Layers, Atmosphere, 14, 1409, https://doi.org/10.3390/atmos14091409, 2023.

Ferrare, R., Hair, J., Hostetler, C., Shingler, T., Burton, S. P., Fenn, M., Clayton, M., Scarino, A. J., Harper, D., Seaman, S., Cook, A., Crosbie, E., Winstead, E., Ziemba, L., Thornhill, L., Robinson, C., Moore, R., Vaughan, M., Sorooshian, A., Schlosser, J. S., Liu, H., Zhang, B., Diskin, G., DiGangi, J., Nowak, J., Choi, Y., Zuidema, P., and Chellappan, S.: Airborne HSRL-2 measurements of elevated aerosol depolarization associated with non-spherical sea salt, Front. Remote Sens., 4, 1143944, https://doi.org/10.3389/frsen.2023.1143944, 2023.

Fishman, J. and Seiler, W.: Correlative nature of ozone and carbon monoxide in the troposphere: Implications for the tropospheric ozone budget, J. Geophys. Res., 88, 3662–3670, https://doi.org/10.1029/JC088iC06p03662, 1983.

Galloway, J. N., Keene, W. C., Artz, R. S., Miller, J. M., Church, T. M., and Knap, A. H.: Processes controlling the concentrations of $SO_4^=$, NO_{-3}, NH_{+4}, H_+, $HCOO_T$ and CH_3COO_T in precipitation on Bermuda, Tellus B, 41, 427–443, https://doi.org/10.1111/j.1600-0889.1989.tb00319.x, 1989.

Gonzalez, M. E., Corral, A. F., Crosbie, E., Dadashazar, H., Diskin, G. S., Edwards, E.-L., Kirschler, S., Moore, R. H., Robinson, C. E., Schlosser, J. S., Shook, M., Stahl, C., Thornhill, K. L., Voigt, C., Winstead, E., Ziemba, L. D., and Sorooshian, A.: Relationships between supermicrometer particle concentrations and cloud water sea salt and dust concentrations: analysis of MONARC and ACTIVATE data, Environ. Sci.-Atmos., 2, 738–752, https://doi.org/10.1039/D2EA00049K, 2022.

Groß, S., Esselborn, M., Weinzierl, B., Wirth, M., Fix, A., and Petzold, A.: Aerosol classification by airborne high spectral resolution lidar observations, Atmos. Chem. Phys., 13, 2487–2505, https://doi.org/10.5194/acp-13-2487-2013, 2013.

Gryspeerdt, E., Povey, A. C., Grainger, R. G., Hasekamp, O., Hsu, N. C., Mulcahy, J. P., Sayer, A. M., and Sorooshian, A.: Uncertainty in aerosol–cloud radiative forcing is driven by clean conditions, Atmos. Chem. Phys., 23, 4115–4122, https://doi.org/10.5194/acp-23-4115-2023, 2023.

Hair, J. W., Hostetler, C. A., Cook, A. L., Harper, D. B., Ferrare, R. A., Mack, T. L., Welch, W., Izquierdo, L. R., and Hovis, F. E.: Airborne High Spectral Resolution Lidar for profiling aerosol optical properties, Appl. Opt., 47, 6734–6752, https://doi.org/10.1364/AO.47.006734, 2008.

Hilario, M. R. A., Crosbie, E., Shook, M., Reid, J. S., Cambaliza, M. O. L., Simpas, J. B. B., Ziemba, L., DiGangi, J. P., Diskin, G. S., Nguyen, P., Turk, F. J., Winstead, E., Robinson, C. E., Wang, J., Zhang, J., Wang, Y., Yoon, S., Flynn, J., Al-

varez, S. L., Behrangi, A., and Sorooshian, A.: Measurement report: Long-range transport patterns into the tropical northwest Pacific during the CAMP²Ex aircraft campaign: chemical composition, size distributions, and the impact of convection, Atmos. Chem. Phys., 21, 3777–3802, https://doi.org/10.5194/acp-21-3777-2021, 2021.

Holben, B. N., Tanré, D., Smirnov, A., Eck, T. F., Slutsker, I., Abuhassan, N., Newcomb, W. W., Schafer, J. S., Chatenet, B., Lavenu, F., Kaufman, Y. J., Castle, J. V., Setzer, A., Markham, B., Clark, D., Frouin, R., Halthore, R., Karneli, A., O'Neill, N. T., Pietras, C., Pinker, R. T., Voss, K., and Zibordi, G.: An emerging ground-based aerosol climatology: Aerosol optical depth from AERONET, J. Geophys. Res.-Atmos., 106, 12067–12097, https://doi.org/10.1029/2001JD900014, 2001.

Holloway, J. S., Jakoubek, R. O., Parrish, D. D., Gerbig, C., Volz-Thomas, A., Schmitgen, S., Fried, A., Wert, B., Henry, B., and Drummond, J. R.: Airborne intercomparison of vacuum ultraviolet fluorescence and tunable diode laser absorption measurements of tropospheric carbon monoxide, J. Geophys. Res., 105, 24251–24261, https://doi.org/10.1029/2000JD900237, 2000.

Honrath, R. E., Owen, R. C., Val Martín, M., Reid, J. S., Lapina, K., Fialho, P., Dziobak, M. P., Kleissl, J., and Westphal, D. L.: Regional and hemispheric impacts of anthropogenic and biomass burning emissions on summertime CO and O_3 in the North Atlantic lower free troposphere, J. Geophys. Res.-Atmos., 109, D24310, https://doi.org/10.1029/2004JD005147, 2004.

Hoppel, W. A., Frick, G. M., and Larson, R. E.: Effect of non-precipitating clouds on the aerosol size distribution in the marine boundary layer, Geophys. Res. Lett., 13, 125–128, https://doi.org/10.1029/GL013i002p00125, 1986.

Horvath, H., Gunter, R. L., and Wilkison, S. W.: Determination of the Coarse Mode of the Atmospheric Aerosol Using Data from a Forward-Scattering Spectrometer Probe, Aerosol Sci. Technol., 12, 964–980, https://doi.org/10.1080/02786829008959407, 1990.

Houghton, H. G.: Problems Connected with the Condensation and Precipitation Processes in the Atmosphere, Bull. Am. Meteorol. Soc., 19, 152–159, https://doi.org/10.1175/1520-0477-19.4.152, 1938.

Huang, Z., Li, M., Bi, J., Shen, X., Zhang, S., and Liu, Q.: Small lidar ratio of dust aerosol observed by Raman-polarization lidar near desert sources, Opt. Express, 31, 16909–16919, https://doi.org/10.1364/OE.484501, 2023.

Illingworth, A., Barker, H., Beljaars, A., Ceccaldi, M., Chepfer, H., Clerbaux, N., Cole, J., Delanoë, J., Domenech, C., Donovan, D., Fukuda, S., Kikuchi, M., Hogan, R., Hünerbein, A., Kollias, P., Kubota, T., Nakajima, T., Nakajima, T., Nishizawa, T., and Zadelhoff, G.-J.: THE EARTHCARE SATELLITE: The next step forward in global measurements of clouds, aerosols, precipitation and radiation, Bull. Am. Meteorol. Soc., 96, 1311–1332, 2015.

Järvinen, E., Kemppinen, O., Nousiainen, T., Kociok, T., Möhler, O., Leisner, T., and Schnaiter, M.: Laboratory investigations of mineral dust near-backscattering depolarization ratios, J. Quant. Spectrosc. Ra., 178, 192–208, https://doi.org/10.1016/j.jqsrt.2016.02.003, 2016.

Kandler, K., Schneiders, K., Ebert, M., Hartmann, M., Weinbruch, S., Prass, M., and Pöhlker, C.: Composition and mixing state of atmospheric aerosols determined by electron mi-

croscopy: method development and application to aged Saharan dust deposition in the Caribbean boundary layer, Atmos. Chem. Phys., 18, 13429–13455, https://doi.org/10.5194/acp-18-13429-2018, 2018.

Kanngießer, F. and Kahnert, M.: Modeling Optical Properties of Non-Cubical Sea-Salt Particles, J. Geophys. Res.-Atmos., 126, e2020JD033674, https://doi.org/10.1029/2020JD033674, 2021.

Keene, W. C., Moody, J. L., Galloway, J. N., Prospero, J. M., Cooper, O. R., Eckhardt, S., and Maben, J. R.: Long-term trends in aerosol and precipitation composition over the western North Atlantic Ocean at Bermuda, Atmos. Chem. Phys., 14, 8119–8135, https://doi.org/10.5194/acp-14-8119-2014, 2014.

Khadir, T., Riipinen, I., Talvinen, S., Heslin-Rees, D., Pöhlker, C., Rizzo, L., Machado, L. A. T., Franco, M. A., Kremper, L. A., Artaxo, P., Petäjä, T., Kulmala, M., Tunved, P., Ekman, A. M. L., Krejci, R., and Virtanen, A.: Sink, Source or Something In-Between? Net Effects of Precipitation on Aerosol Particle Populations, Geophys. Res. Lett., 50, e2023GL104325, https://doi.org/10.1029/2023GL104325, 2023.

Kim, Y., Sievering, H., and Boatman, J.: Volume and surface area size distribution, water mass and model fitting of GCE/-CASE/WATOX marine aerosols, Global Biogeochem. Cy., 4, 165–177, https://doi.org/10.1029/GB004i002p00165, 1990.

Kirschler, S., Voigt, C., Anderson, B., Campos Braga, R., Chen, G., Corral, A. F., Crosbie, E., Dadashazar, H., Ferrare, R. A., Hahn, V., Hendricks, J., Kaufmann, S., Moore, R., Pöhlker, M. L., Robinson, C., Scarino, A. J., Schollmayer, D., Shook, M. A., Thornhill, K. L., Winstead, E., Ziemba, L. D., and Sorooshian, A.: Seasonal updraft speeds change cloud droplet number concentrations in low-level clouds over the western North Atlantic, Atmos. Chem. Phys., 22, 8299–8319, https://doi.org/10.5194/acp-22-8299-2022, 2022.

Kirschler, S., Voigt, C., Anderson, B. E., Chen, G., Crosbie, E. C., Ferrare, R. A., Hahn, V., Hair, J. W., Kaufmann, S., Moore, R. H., Painemal, D., Robinson, C. E., Sanchez, K. J., Scarino, A. J., Shingler, T. J., Shook, M. A., Thornhill, K. L., Winstead, E. L., Ziemba, L. D., and Sorooshian, A.: Overview and statistical analysis of boundary layer clouds and precipitation over the western North Atlantic Ocean, Atmos. Chem. Phys., 23, 10731–10750, https://doi.org/10.5194/acp-23-10731-2023, 2023.

Le Blond, J. S., Woskie, S., Horwell, C. J., and Williamson, B. J.: Particulate matter produced during commercial sugarcane harvesting and processing: A respiratory health hazard?, Atmos. Environ., 149, 34–46, https://doi.org/10.1016/j.atmosenv.2016.11.012, 2017.

Logan, J. A., Prather, M. J., Wofsy, S. C., and McElroy, M. B.: Tropospheric chemistry: A global perspective, J. Geophys. Res.-Ocean., 86, 7210–7254, https://doi.org/10.1029/JC086iC08p07210, 1981.

Luria, M., Van Valin, C. C., Galloway, J. N., Keene, W. C., Wellman, D. L., Sievering, H., and Boatman, J. F.: The relationship between dimethyl sulfide and particulate sulfate in the mid-atlantic ocean atmosphere, Atmos. Environ., 23, 139–147, https://doi.org/10.1016/0004-6981(89)90106-6, 1989.

Lynch, P., Reid, J. S., Westphal, D. L., Zhang, J., Hogan, T. F., Hyer, E. J., Curtis, C. A., Hegg, D. A., Shi, Y., Campbell, J. R., Rubin, J. I., Sessions, W. R., Turk, F. J., and Walker, A. L.: An 11-year global gridded aerosol optical thickness reanalysis (v1.0) for at-

mospheric and climate sciences, Geosci. Model Dev., 9, 1489–1522, https://doi.org/10.5194/gmd-9-1489-2016, 2016.

Mardi, A. H., Dadashazar, H., Painemal, D., Shingler, T., Seaman, S. T., Fenn, M. A., Hostetler, C. A., and Sorooshian, A.: Biomass Burning Over the United States East Coast and Western North Atlantic Ocean: Implications for Clouds and Air Quality, J. Geophys. Res.-Atmos., 126, e2021JD034916, https://doi.org/10.1029/2021JD034916, 2021.

Merrill, J. T., Moody, J. L., Oltmans, S. J., and Levy II, H.: Meteorological analysis of tropospheric ozone profiles at Bermuda, J. Geophys. Res.-Atmos., 101, 29201–29211, https://doi.org/10.1029/95JD03432, 1996.

Milne, P. J., Prados, A. I., Dickerson, R. R., Doddridge, B. G., Riemer, D. D., Zika, R. G., Merrill, J. T., and Moody, J. L.: Nonmethane hydrocarbon mixing ratios in continental outflow air from eastern North America: Export of ozone precursors to Bermuda, J. Geophys. Res.-Atmos., 105, 9981–9990, https://doi.org/10.1029/1999JD901117, 2000.

Moody, J. L., Oltmans, S. J., Levy II, H., and Merrill, J. T.: Transport climatology of tropospheric ozone: Bermuda, 1988–1991, J. Geophys. Res.-Atmos., 100, 7179–7194, https://doi.org/10.1029/94JD02830, 1995.

Moody, J. L., Keene, W. C., Cooper, O. R., Voss, K. J., Aryal, R., Eckhardt, S., Holben, B., Maben, J. R., Izaguirre, M. A., and Galloway, J. N.: Flow climatology for physicochemical properties of dichotomous aerosol over the western North Atlantic Ocean at Bermuda, Atmos. Chem. Phys., 14, 691–717, https://doi.org/10.5194/acp-14-691-2014, 2014.

Moore, R. H., Wiggins, E. B., Ahern, A. T., Zimmerman, S., Montgomery, L., Campuzano Jost, P., Robinson, C. E., Ziemba, L. D., Winstead, E. L., Anderson, B. E., Brock, C. A., Brown, M. D., Chen, G., Crosbie, E. C., Guo, H., Jimenez, J. L., Jordan, C. E., Lyu, M., Nault, B. A., Rothfuss, N. E., Sanchez, K. J., Schueneman, M., Shingler, T. J., Shook, M. A., Thornhill, K. L., Wagner, N. L., and Wang, J.: Sizing response of the Ultra-High Sensitivity Aerosol Spectrometer (UHSAS) and Laser Aerosol Spectrometer (LAS) to changes in submicron aerosol composition and refractive index, Atmos. Meas. Tech., 14, 4517–4542, https://doi.org/10.5194/amt-14-4517-2021, 2021.

Muhs, D. R., Budahn, J. R., Prospero, J. M., Skipp, G., and Herwitz, S. R.: Soil genesis on the island of Bermuda in the Quaternary: The importance of African dust transport and deposition, J. Geophys. Res.-Earth, 117, F03025, https://doi.org/10.1029/2012JF002366, 2012.

Oltmans, S. J. and Levy, H.: Seasonal cycle of surface ozone over the western North Atlantic, Nature, 358, 392–394, https://doi.org/10.1038/358392a0, 1992.

Painemal, D., Corral, A. F., Sorooshian, A., Brunke, M. A., Chellappan, S., Afzali Gorooh, V., Ham, S.-H., O'Neill, L., Smith Jr., W. L., Tselioudis, G., Wang, H., Zeng, X., and Zuidema, P.: An Overview of Atmospheric Features Over the Western North Atlantic Ocean and North American East Coast – Part 2: Circulation, Boundary Layer, and Clouds, J. Geophys. Res.-Atmos., 126, e2020JD033423, https://doi.org/10.1029/2020JD033423, 2021.

PéTron, G., Granier, C., Khattatov, B., Lamarque, J.-F., Yudin, V., Müller, J.-F., and Gille, J.: Inverse modeling of carbon monoxide surface emissions using Climate Monitoring and Diagnostics

Laboratory network observations, J. Geophys. Res.-Atmos., 107, 4761, https://doi.org/10.1029/2001JD001305, 2002.

Porter, J. N. and Clarke, A. D.: Aerosol size distribution models based on in situ measurements, J. Geophys. Res.-Atmos., 102, 6035–6045, https://doi.org/10.1029/96JD03403, 1997.

Pringle, K. J., Tost, H., Pozzer, A., Pöschl, U., and Lelieveld, J.: Global distribution of the effective aerosol hygroscopicity parameter for CCN activation, Atmos. Chem. Phys., 10, 5241–5255, https://doi.org/10.5194/acp-10-5241-2010, 2010.

Reid, J. S., Jonsson, H. H., Smith, M. H., and Smirnov, A.: Evolution of the vertical profile and flux of large sea-salt particles in a coastal zone, J. Geophys. Res.-Atmos., 106, 12039–12053, https://doi.org/10.1029/2000JD900848, 2001.

Reid, J. S, Brooks, B., Crahan, K. K., Hegg, D. A., Eck, T. F., O'Neill, N., de Leeuw, G., Reid, E. A., and Anderson, K. D.: Reconciliation of coarse mode sea-salt aerosol particle size measurements and parameterizations at a subtropical ocean receptor site, J. Geophys. Res.-Atmos., 111, D02202, https://doi.org/10.1029/2005JD006200, 2006.

Robson, J., Sutton, R. T., Archibald, A., Cooper, F., Christensen, M., Gray, L. J., Holliday, N. P., Macintosh, C., McMillan, M., Moat, B., Russo, M., Tilling, R., Carslaw, K., Desbruyères, D., Embury, O., Feltham, D. L., Grosvenor, D. P., Josey, S., King, B., Lewis, A., McCarthy, G. D., Merchant, C., New, A. L., O'Reilly, C. H., Osprey, S. M., Read, K., Scaife, A., Shepherd, A., Sinha, B., Smeed, D., Smith, D., Ridout, A., Woollings, T., and Yang, M.: Recent multivariate changes in the North Atlantic climate system, with a focus on 2005–2016, Int. J. Climatol., 38, 5050–5076, https://doi.org/10.1002/joc.5815, 2018.

Rolph, G., Stein, A., and Stunder, B.: Real-time Environmental Applications and Display sYstem: READY, Environ. Model. Softw., 95, 210–228, https://doi.org/10.1016/j.envsoft.2017.06.025, 2017.

Scarino, A. J., Obland, M. D., Fast, J. D., Burton, S. P., Ferrare, R. A., Hostetler, C. A., Berg, L. K., Lefer, B., Haman, C., Hair, J. W., Rogers, R. R., Butler, C., Cook, A. L., and Harper, D. B.: Comparison of mixed layer heights from airborne high spectral resolution lidar, ground-based measurements, and the WRF-Chem model during CalNex and CARES, Atmos. Chem. Phys., 14, 5547–5560, https://doi.org/10.5194/acp-14-5547-2014, 2014.

Schum, S. K., Zhang, B., Džepina, K., Fialho, P., Mazzoleni, C., and Mazzoleni, L. R.: Molecular and physical characteristics of aerosol at a remote free troposphere site: implications for atmospheric aging, Atmos. Chem. Phys., 18, 14017–14036, https://doi.org/10.5194/acp-18-14017-2018, 2018.

Seibert, P., Beyrich, F., Gryning, S.-E., Joffre, S., Rasmussen, A., and Tercier, P.: Review and intercomparison of operational methods for the determination of the mixing height, Atmos. Environ., 34, 1001–1027, https://doi.org/10.1016/S1352-2310(99)00349-0, 2000.

Sevimoglu, O. and Rogge, W. F.: Organic Compound Concentrations of Size-Segregated PM_{10} during Sugarcane Burning and Growing Seasons at a Rural and an Urban Site in Florida, USA, Aerosol Air Qual. Res., 15, 1720–1736, https://doi.org/10.4209/aaqr.2015.02.0069, 2015.

Shilling, J. E., Pekour, M. S., Fortner, E. C., Artaxo, P., de Sá, S., Hubbe, J. M., Longo, K. M., Machado, L. A. T., Martin, S. T., Springston, S. R., Tomlinson, J., and Wang, J.: Aircraft obser-

vations of the chemical composition and aging of aerosol in the Manaus urban plume during GoAmazon 2014/5, Atmos. Chem. Phys., 18, 10773–10797, https://doi.org/10.5194/acp-18-10773-2018, 2018.

Shingler, T., Crosbie, E., Ortega, A., Shiraiwa, M., Zuend, A., Beyersdorf, A., Ziemba, L., Anderson, B., Thornhill, L., Perring, A. E., Schwarz, J. P., Campazano-Jost, P., Day, D. A., Jimenez, J. L., Hair, J. W., Mikoviny, T., Wisthaler, A., and Sorooshian, A.: Airborne characterization of subsaturated aerosol hygroscopicity and dry refractive index from the surface to 6.5 km during the SEAC4RS campaign, J. Geophys. Res.-Atmos., 121, 4188–4210, https://doi.org/10.1002/2015JD024498, 2016a.

Shingler, T., Sorooshian, A., Ortega, A., Crosbie, E., Wonaschütz, A., Perring, A. E., Beyersdorf, A., Ziemba, L., Jimenez, J. L., Campuzano-Jost, P., Mikoviny, T., Wisthaler, A., and Russell, L. M.: Ambient observations of hygroscopic growth factor and f (RH) below 1: Case studies from surface and airborne measurements, J. Geophys. Res.-Atmos., 121, 13661–13677, https://doi.org/10.1002/2016JD025471, 2016b.

Smirnov, A., Holben, B. N., Kaufman, Y. J., Dubovik, O., Eck, T. F., Slutsker, I., Pietras, C., and Halthore, R. N.: Optical Properties of Atmospheric Aerosol in Maritime Environments, J. Atmos. Sci., 59, 501–523, https://doi.org/10.1175/1520-0469(2002)059<0501:OPOAAI>2.0.CO;2, 2002.

Sorooshian, A., Murphy, S. M., Hersey, S., Bahreini, R., Jonsson, H., Flagan, R. C., and Seinfeld, J. H.: Constraining the contribution of organic acids and AMS m/z 44 to the organic aerosol budget: On the importance of meteorology, aerosol hygroscopicity, and region, Geophys. Res. Lett., 37, L21807, https://doi.org/10.1029/2010GL044951, 2010.

Sorooshian, A., Anderson, B., Bauer, S. E., Braun, R. A., Cairns, B., Crosbie, E., Dadashazar, H., Diskin, G., Ferrare, R., Flagan, R. C., Hair, J., Hostetler, C., Jonsson, H. H., Kleb, M. M., Liu, H., MacDonald, A. B., McComiskey, A., Moore, R., Painemal, D., Russell, L. M., Seinfeld, J. H., Shook, M., Smith, W. L., Thornhill, K., Tselioudis, G., Wang, H., Zeng, X., Zhang, B., Ziemba, L., and Zuidema, P.: Aerosol–Cloud–Meteorology Interaction Airborne Field Investigations: Using Lessons Learned from the U.S. West Coast in the Design of ACTIVATE off the U.S. East Coast, Bull. Am. Meteorol. Soc., 100, 1511–1528, https://doi.org/10.1175/BAMS-D-18-0100.1, 2019.

Sorooshian, A., Corral, A. F., Braun, R. A., Cairns, B., Crosbie, E., Ferrare, R., Hair, J., Kleb, M. M., Hossein Mardi, A., Maring, H., McComiskey, A., Moore, R., Painemal, D., Scarino, A. J., Schlosser, J., Shingler, T., Shook, M., Wang, H., Zeng, X., Ziemba, L., and Zuidema, P.: Atmospheric Research Over the Western North Atlantic Ocean Region and North American East Coast: A Review of Past Work and Challenges Ahead, J. Geophys. Res.-Atmos., 125, e2019JD031626, https://doi.org/10.1029/2019JD031626, 2020.

Sorooshian, A., Alexandrov, M. D., Bell, A. D., Bennett, R., Betito, G., Burton, S. P., Buzanowicz, M. E., Cairns, B., Chemyakin, E. V., Chen, G., Choi, Y., Collister, B. L., Cook, A. L., Corral, A. F., Crosbie, E. C., van Diedenhoven, B., DiGangi, J. P., Diskin, G. S., Dmitrovic, S., Edwards, E.-L., Fenn, M. A., Ferrare, R. A., van Gilst, D., Hair, J. W., Harper, D. B., Hilario, M. R. A., Hostetler, C. A., Jester, N., Jones, M., Kirschler, S., Kleb, M. M., Kusterer, J. M., Leavor, S., Lee, J. W., Liu, H., McCauley, K., Moore, R. H., Nied, J., Notari, A., Nowak, J. B., Painemal,

D., Phillips, K. E., Robinson, C. E., Scarino, A. J., Schlosser, J. S., Seaman, S. T., Seethala, C., Shingler, T. J., Shook, M. A., Sinclair, K. A., Smith Jr., W. L., Spangenberg, D. A., Stamnes, S. A., Thornhill, K. L., Voigt, C., Vömel, H., Wasilewski, A. P., Wang, H., Winstead, E. L., Zeider, K., Zeng, X., Zhang, B., Ziemba, L. D., and Zuidema, P.: Spatially coordinated airborne data and complementary products for aerosol, gas, cloud, and meteorological studies: the NASA ACTIVATE dataset, Earth Syst. Sci. Data, 15, 3419–3472, https://doi.org/10.5194/essd-15-3419-2023, 2023.

Stein, A. F., Draxler, R. R., Rolph, G. D., Stunder, B. J. B., Cohen, M. D., and Ngan, F.: NOAA's HYSPLIT Atmospheric Transport and Dispersion Modeling System, Bull. Am. Meteorol. Soc., 96, 2059–2077, https://doi.org/10.1175/BAMS-D-14-00110.1, 2015.

Thornhill, K. L., Anderson, B. E., Barrick, J. D. W., Bagwell, D. R., Friesen, R., and Lenschow, D. H.: Air motion intercomparison flights during Transport and Chemical Evolution in the Pacific (TRACE-P)/ACE-ASIA, J. Geophys. Res.-Atmos., 108, D208783, https://doi.org/10.1029/2002JD003108, 2003.

Todd, D. L., Keene, W. C., Moody, J. L., Maring, H., and Galloway, J. N.: Effects of wet deposition on optical properties of the atmosphere over Bermuda and Barbados, J. Geophys. Res.-Atmos., 108, D34099, https://doi.org/10.1029/2001JD001084, 2003.

Virtanen, P., Gommers, R., Oliphant, T. E., Haberland, M., Reddy, T., Cournapeau, D., Burovski, E., Peterson, P., Weckesser, W., Bright, J., van der Walt, S. J., Brett, M., Wilson, J., Millman, K. J., Mayorov, N., Nelson, A. R. J., Jones, E., Kern, R., Larson, E., Carey, C. J., Polat, Ý., Feng, Y., Moore, E. W., VanderPlas, J., Laxalde, D., Perktold, J., Cimrman, R., Henriksen, I., Quintero, E. A., Harris, C. R., Archibald, A. M., Ribeiro, A. H., Pedregosa, F., and van Mulbregt, P.: SciPy 1.0: fundamental algorithms for scientific computing in Python, Nat. Method., 17, 261–272, https://doi.org/10.1038/s41592-019-0686-2, 2020.

Vömel, H., Sorooshian, A., Robinson, C., Shingler, T. J., Thornhill, K. L., and Ziemba, L. D.: Dropsonde observations during the Aerosol Cloud meTeorology Interactions oVer the western ATlantic Experiment, Sci. Data, 10, 753, https://doi.org/10.1038/s41597-023-02647-5, 2023.

Wei, Y., Shrestha, R., Pal, S., Gerken, T., Feng, S., McNelis, J., Singh, D., Thornton, M. M., Boyer, A. G., Shook, M. A., Chen, G., Baier, B. C., Barkley, Z. R., Barrick, J. D., Bennett, J. R., Browell, E. V., Campbell, J. F., Campbell, L. J., Choi, Y., Collins, J., Dobler, J., Eckl, M., Fiehn, A., Fried, A., Digangi, J. P., Barton-Grimley, R., Halliday, H., Klausner, T., Kooi, S., Kostinek, J., Lauvaux, T., Lin, B., McGill, M. J., Meadows, B., Miles, N. L., Nehrir, A. R., Nowak, J. B., Obland, M., O'Dell, C., Fao, R. M. P., Richardson, S. J., Richter, D., Roiger, A., Sweeney, C., Walega, J., Weibring, P., Williams, C. A., Yang, M. M., Zhou, Y., and Davis, K. J.: Atmospheric Carbon and Transport – America (ACT-America) Data Sets: Description, Management, and Delivery, Earth Space Sci., 8, e2020EA001634, https://doi.org/10.1029/2020EA001634, 2021.

Wolff, G. T., Ruthkosky, M. S., Stroup, D. P., Korsog, P. E., Ferman, M. A., Wendel, G. J., and Stedman, D. H.: Measurements of SO_x, NO_x and aerosol species on Bermuda, Atmos. Environ., 20, 1229–1239, https://doi.org/10.1016/0004-6981(86)90158-7, 1986.

Xiao, Q., Zhang, J., Wang, Y., Ziemba, L. D., Crosbie, E., Winstead, E. L., Robinson, C. E., DiGangi, J. P., Diskin, G. S., Reid, J. S., Schmidt, K. S., Sorooshian, A., Hilario, M. R. A., Woods, S., Lawson, P., Stamnes, S. A., and Wang, J.: New particle formation in the tropical free troposphere during CAMP²Ex: statistics and impact of emission sources, convective activity, and synoptic conditions, Atmos. Chem. Phys., 23, 9853–9871, https://doi.org/10.5194/acp-23-9853-2023, 2023.

Zawadowicz, M. A., Suski, K., Liu, J., Pekour, M., Fast, J., Mei, F., Sedlacek, A. J., Springston, S., Wang, Y., Zaveri, R. A., Wood, R., Wang, J., and Shilling, J. E.: Aircraft measurements of aerosol and trace gas chemistry in the eastern North Atlantic, Atmos. Chem. Phys., 21, 7983–8002, https://doi.org/10.5194/acp-21-7983-2021, 2021.

Zhang, Q., Alfarra, M. R., Worsnop, D. R., Allan, J. D., Coe, H., Canagaratna, M. R., and Jimenez, J. L.: Deconvolution and Quantification of Hydrocarbon-like and Oxygenated Organic Aerosols Based on Aerosol Mass Spectrometry, Environ. Sci. Technol., 39, 4938–4952, https://doi.org/10.1021/es048568l, 2005.

Zheng, G., Wang, Y., Wood, R., Jensen, M. P., Kuang, C., McCoy, I. L., Matthews, A., Mei, F., Tomlinson, J. M., Shilling, J. E., Zawadowicz, M. A., Crosbie, E., Moore, R., Ziemba, L., Andreae, M. O., and Wang, J.: New particle formation in the remote marine boundary layer, Nat. Commun., 12, 527, https://doi.org/10.1038/s41467-020-20773-1, 2021.

Ziemba, L. D., Lee Thornhill, K., Ferrare, R., Barrick, J., Beyersdorf, A. J., Chen, G., Crumeyrolle, S. N., Hair, J., Hostetler, C., Hudgins, C., Obland, M., Rogers, R., Scarino, A. J., Winstead, E. L., and Anderson, B. E.: Airborne observations of aerosol extinction by in situ and remote-sensing techniques: Evaluation of particle hygroscopicity, Geophys. Res. Lett., 40, 417–422, https://doi.org/10.1029/2012GL054428, 2013.

Zuidema, P., III, A., Flynn, C., Springston, S., Delgadillo, R., Zhang, J., Aiken, A., Koontz, A., and Muradyan, P.: The Ascension Island Boundary Layer in the Remote Southeast Atlantic is Often Smoky, Geophys. Res. Lett., 45, 4456–4465, https://doi.org/10.1002/2017gl076926, 2017.